Quenching of weak interactions in nucleon matter

S. Cowell and V. R. Pandharipande
Department of Physics, University of Illinois at Urbana-Champaign, 1110 West Green Street, Urbana, Illinois 61801
(Received 5 November 2002; published 28 March 2003)

We have calculated the one-body Fermi and Gamow-Teller charge-current and vector and axial-vector neutral-current nuclear matrix elements in nucleon matter at densities of 0.08, 0.16, and 0.24 fm^{-3} and proton fractions ranging from 0.2 to 0.5. The correlated states for nucleon matter are obtained by operating on Fermi-gas states by a symmetrized product of pair correlation operators determined from variational calculations with the Argonne-v18 and Urbana-IX two- and three-nucleon interactions. The squares of the charge-current matrix elements are found to be quenched by 20–25 % by the short-range correlations in nucleon matter. Most of the quenching is due to spin-isospin correlations induced by the pion exchange interactions which change the isospins and spins of the nucleons. A large part of it can be related to the probability for a spin-up proton quasiparticle to be a bare spin-up/down proton/neutron. Within the interval considered, the charge-current matrix elements do not have significant dependence on the matter density, proton fraction, and magnitudes of nucleon momenta; however, they do depend on momentum transfer. The neutral-current matrix elements have a significant dependence on the proton fraction. We also calculate the matrix elements of the nuclear Hamiltonian in the same correlated basis. These provide relatively mild effective interactions that give the variational energies in the Hartree-Fock approximation. The calculated two-nucleon effective interaction describes the spin-isospin susceptibilities of nuclear and neutron matter fairly accurately. However terms greater than or equal to three-body terms are necessary to reproduce the compressibility. Realistic calculations of weak interaction rates in nucleon matter can presumably be carried out using the effective operators and interactions studied here. All presented results use the simple two-body cluster approximation to calculate the correlated basis matrix elements. This allows for a clear discussion of the physical effects in the effective operators and interactions.

DOI: 10.1103/PhysRevC.67.035504 PACS number(s): 21.30.Fe, 23.40.Hc, 26.50.+x

I. INTRODUCTION

Weak interactions in nucleon matter occur during the β-decay of nuclei, electron and muon capture reactions, neutrino-nucleus scattering, and in various astrophysical environments, such as evolving stars, neutron stars, and supernovas. They have been studied since Fermi proposed the first theory of β decay in 1934. Recently there has been much interest in weak interactions in the sun [1,2], those of ^{12}C, and ^{16}O due to their use in neutrino detectors searching for neutrino oscillations [3–6], and in interactions of neutrinos with dense matter in neutron stars and supernovas [7]. Low energy weak interactions proceed mainly via the nuclear matrix elements of the following four one-body operators:

$$O_F = \sum_i O_F(i) = \sum_i \tau_i^+ e^{i\mathbf{q}\cdot\mathbf{r}_i}, \tag{1}$$

$$\mathbf{O}_{GT} = g_A \sum_i \mathbf{O}_{GT}(i) = g_A \sum_i \tau_i^+ \boldsymbol{\sigma}_i e^{i\mathbf{q}\cdot\mathbf{r}_i}, \tag{2}$$

$$O_{NV} = \sum_i O_{NV}(i) = \sum_i \left(-\sin^2\theta_W + \frac{1}{2}(1 - 2\sin^2\theta_W)\tau_i^z \right) e^{i\mathbf{q}\cdot\mathbf{r}_i}, \tag{3}$$

$$\mathbf{O}_{NA} = g_A \sum_i \mathbf{O}_{NA}(i) = g_A \sum_i \frac{1}{2}\tau_i^z \boldsymbol{\sigma}_i e^{i\mathbf{q}\cdot\mathbf{r}_i}. \tag{4}$$

Here i is the nucleon number label and $\mathbf{q}$ is the momentum given by the weak boson to the nucleon. The Fermi coupling constant multiplying these operators is omitted for brevity, θ_W is the electroweak mixing angle, and g_A is the ratio of the weak axial vector and Fermi coupling constants of the nucleon. The four operators are called Fermi (F), Gamow-Teller (GT), neutral-vector (NV), and neutral-axial-vector (NA). In the nonrelativistic domain, neglecting weak pair currents, the interaction of low energy neutrinos with nuclei and nucleon matter and nuclear β-decay rates are proportional to the square of the matrix elements of these operators between initial and final nuclear states.

Due to the strong forces, nuclear wave functions are highly correlated [8,9], and it is difficult to calculate the nuclear matrix elements. Using quantum Monte Carlo and Faddeev methods to calculate nuclear wave functions from realistic models of nuclear forces, the β-decay matrix elements have been calculated for light nuclei with $A \leqslant 7$ [10,11]. The calculated values for ^{3}H, ^{6}He, and ^{7}Be are within 5% of the observed, and better agreement is obtained after including weak pair currents. The weak muon capture by ^{3}He has also been calculated [12] with realistic wave functions with similar success.

However, complete many-body calculations are not yet possible for nuclei such as ^{12}C and heavier, as well as for nucleon matter. Most studies of weak interactions in these systems use effective interactions and shell-model and Fermi-gas wave functions in finite nuclei and nucleon matter, respectively. The random phase approximation is commonly used. The pioneering work on GT transitions has been re-

viewed by Arima *et. al* [13]. Some of the recent works are in ^{12}C [14,15], in pf shell [16,17], and in neutron stars and supernovas [18]. Typically the calculated rate of weak interactions is larger than observed; for example, a factor of ~ 0.6 brings the calculated pf shell GT transition rates in agreement with experiment. Recent Liquid Scintillating Neutrino Detector (LSND) results of charged current reaction cross sections of ν_e [4] and ν_μ [5] on ^{12}C are lower than the theoretical expectations by up to 20%.

This is not surprising since effective operators that take into account the effects of short range correlations, and not the bare operators given by Eqs. (1)–(4), must be used along with effective interactions as is well known from the works of Arima and collaborators [13]. In nuclei near the line of stability the observed spectra and β-decay rates have been used to model the effective interactions and operators, but for neutron stars and supernovas matter we have to calculate them from realistic models of nuclear forces. In pf shell and heavier nuclei, the effective interaction is also obtained from bare forces [19].

There are several ways to obtain consistent sets of effective operators and interactions starting from a bare nuclear Hamiltonian. For example, one can introduce a model space and employ the Lee-Suzuki similarity transformation [20] as in the no core shell model type approach [21]. In this theory the effective operators and interactions take into account the truncated Hilbert space. They are used in the retained model space to predict the observables. In the present work we use the correlated basis (CB) approach [22,23], evolved out of variational theories of quantum liquids [24]. In this theory the uncorrelated shell-model or Fermi-gas states are transformed by correlation operators to CB states without truncation of the Hilbert space. The effective operators and interactions are matrix elements of the bare quantities in the CB states; they take into account the effects of short-range correlations. The correlation operators are chosen such that the nuclear interactions are relatively mild in the CB. Observables are calculated using standard many-body perturbation theory methods in CB.

Here we focus on weak interactions in nucleon matter. In variational calculations [9], the nuclear matter wave functions are approximated with correlated states:

$$\Psi_X = \left(\mathcal{S} \prod_{i<j} F_{ij} \right) \Phi_X , \tag{5}$$

where Φ_X are uncorrelated Fermi-gas (FG) states and F_{ij} are pair correlation operators. The $\mathcal{S}\Pi$ denotes a symmetrized product necessary because F_{ij} and F_{ik} do not commute. One can also relate uncorrelated shell-model states to correlated states in a similar way. The correlated states obtained from Eq. (5) are not orthogonal; we assume that they are orthonormalized using a combination of Löwdin and Schmidt transformations [23] preserving the diagonal matrix elements of the Hamiltonian. However, the orthonormalization corrections are of higher order than those considered here.

Let $|X\rangle$ denote the orthonormal correlated states. The effective interactions in the CB perturbation theory are defined such that

$$\langle X|H|Y\rangle = \langle \Phi_X | H_0 + H_I | \Phi_Y \rangle , \tag{6}$$

$$H_0 = \sum_i -\frac{\hbar^2}{2m} \nabla_i^2 , \tag{7}$$

$$H_I = \sum_{i<j} v_{ij}^{CB} + \sum_{i<j<k} V_{ijk}^{CB} + \cdots . \tag{8}$$

Here H is the nuclear Hamiltonian containing realistic two- and possibly three-nucleon interactions. Even when H has only two-body interactions, the CB H_I can have three- and higher-body terms. Since the correlated states are expected to be close to the eigenstates of H, the nondiagonal matrix elements $\langle X \neq Y|H|Y\rangle$ are small. This implies that the CB effective interactions can be used in perturbation expansions based on the Hartree-Fock approximation. However, the first-order results are often not sufficiently accurate. The product of pair correlation operators [Eq. (5)] cannot transform the uncorrelated states into the exact eigenstates of H. CB calculations of the optical potential of nucleons in nuclear matter [25] including up to second-order terms in H_I, and of the response of nucleon matter to electromagnetic probes including correlated particle-hole rescattering [26], have been relatively successful. In these works, as well as here, the three- and higher-body effective interactions are neglected.

In the present work we use the static pair correlation operator:

$$F_{ij} = \sum_{p=1,6} f^p(r_{ij}) O_{ij}^p , \tag{9}$$

$$O_{ij}^{p=1,6} = 1, \boldsymbol{\tau}_i \cdot \boldsymbol{\tau}_j, \boldsymbol{\sigma}_i \cdot \boldsymbol{\sigma}_j, \boldsymbol{\tau}_i \cdot \boldsymbol{\tau}_j \boldsymbol{\sigma}_i \cdot \boldsymbol{\sigma}_j, S_{ij}, \boldsymbol{\tau}_i \cdot \boldsymbol{\tau}_j S_{ij} . \tag{10}$$

In place of the $p=1,6$ superscripts we often use the letters c, τ, σ, $\sigma\tau$, t, and $t\tau$ to denote the radial functions associated with these operators. For example,

$$f^{p=1,6}(r_{ij}) \equiv f_{ij}^c, f_{ij}^\tau, f_{ij}^\sigma, f_{ij}^{\sigma\tau}, f_{ij}^t, f_{ij}^{t\tau} . \tag{11}$$

F_{ij} is obtained by minimizing the energy of symmetric nuclear matter at density $\rho = \rho_n + \rho_p$ using hypernetted and operator chain summation methods [9,27]. The results of the latest [27] variational calculations are briefly summarized in Sec. VI for completeness. The Argonne v18 two-nucleon [28] and Urbana IX three-nucleon [29] interactions are used in these nuclear matter calculations, in studies of weak interactions of light nuclei [10,11], and in the present work. However, improved models of V_{ijk} are now available [30]. The variational calculations of nucleon matter also include two spin-orbit terms in F_{ij}, which are omitted here for simplicity. The variationally optimized F_{ij} can depend on the proton fraction x_p. However, this dependence seems to be relatively weak. The effective interaction obtained from F_{ij} in symmetric nuclear matter gives a fair description of the spin susceptibility of pure neutron matter.

Matrix elements of operators between CB states are generally calculated using cluster expansions [31]. We begin

with the simplest, lowest-order two-nucleon cluster approximation to study the general properties of the weak one-body effective operators and of the two-body interactions in CB for nucleon matter at densities $\rho=0.08$, 0.16, and 0.24 fm^{-3} and for proton fractions $x_p=\rho_p/\rho=$ 0.2, 0.3, 0.4, and 0.5. In this density range the contributions of clusters with $\geqslant 3$ nucleons to the energy of symmetric nuclear matter increases from 10% to 30% of that of the two-body [27]; thus the present results have only qualitative significance. We study the density, proton fraction, and momentum dependence of the operators and the interactions.

Due to correlations and weak pair currents, the effective weak current operators have two- and many-body terms in addition to the leading one-body term we consider here. The lowest-order (in cluster expansion) effective one-body F, GT, and neutral-current operators are calculated and their results are presented in Secs. II–V. As expected, the one-body CB matrix elements are smaller in magnitude than those in the FG states. The dominant term responsible for the quenching arises from pion exchange interactions that change the isospins and spins of the nucleons. In the FG wave function, a nucleon in the single-particle state $e^{i\mathbf{k}\cdot\mathbf{r}}\chi_{n\uparrow}$, for example, is a spin $\uparrow$ neutron with unit probability. This probability is reduced in the CB state by the spin-isospin correlation operators acting on the FG state. In contrast, the spin-isospin independent spatial correlations induced by the repulsive core in the two-nucleon interaction increase the magnitude of F, GT, and NA matrix elements; however, they quench the neutron NV. The CB matrix elements of the charge-current operators are found to have a rather small dependence on the matter density and x_p within the range considered. They depend primarily on the momentum transfer q, and only slightly on the initial or final nucleon momentum. In addition to these, the neutral-current matrix elements also depend on x_p. The proton NV matrix element is an exception; it has large cancellations and depends on all the relevant variables.

The squares of the F and GT matrix elements in CB states are ~ 0.8 and 0.75 times those in FG states at small values of q. Thus the present zeroth-order (in CB H_1) two-body cluster calculation predicts a quenching of low energy weak transitions in nuclei and nucleon matter by ~ 20–$25\,\%$. It is likely that higher-order effects will further reduce the matrix elements and increase the quenching. For example, the occupation probability of states with momenta $\lesssim k_F$ is ~ 0.9 in CB states, and it decreases to ~ 0.8 on including second-order $H_{\rm I}$ corrections [32]. In order to obtain quantitative results, it will be necessary to include contributions of greater than or equal to three-body clusters to the CB matrix elements neglected in this initial study. This has been done for symmetric nuclear matter [25] with operator chain summation techniques; however, they are difficult to use in matter with $x_p\neq 0.5$. Three-body cluster contributions in asymmetric matter can now be calculated using the recently developed matrix methods [27].

The results for the CB two-nucleon interaction are presented in Sec. VI. It gives a fair description of the spin-isospin susceptibilities of nucleon matter used to determine the effective interactions in the Landau-Migdal scheme [7]. It also has the typical features of the effective interactions used in existing calculations of weak interactions in nucleon matter [18]. If we assume that the calculations with effective interactions are implicitly using CB states, then their results should be reduced by a factor of ~ 0.75 to take into account the quenching of the F and GT matrix elements by short-range correlations. Attempts to calculate the weak interaction rates in nucleon matter with the effective operators and CB interaction presented here are in progress.

II. CORRELATED BASIS FERMI MATRIX ELEMENT

Let $|I\rangle$ and $|F\rangle$ denote the normalized correlated states obtained by operating on the FG states $|\Phi_I\rangle$ and $|\Phi_F\rangle$ by the correlation operator $\mathcal{S}\Pi F_{ij}$. The CB Fermi matrix elements are given by

$$\langle F|O_F|I\rangle=\frac{\langle\Phi_F|[\mathcal{S}\Pi F_{ij}]O_F[\mathcal{S}\Pi F_{ij}]|\Phi_I\rangle}{\sqrt{\langle\Phi_F|[\mathcal{S}\Pi F_{ij}]^2|\Phi_F\rangle\langle\Phi_I|[\mathcal{S}\Pi F_{ij}]^2|\Phi_I\rangle}}, \tag{12}$$

apart from the orthogonality corrections [23] neglected here. The corresponding uncorrelated, FG matrix element (FGME) is $\langle\Phi_F|O_F|\Phi_I\rangle$. It is nonzero only when the occupation numbers of the states Φ_I and Φ_F differ by only one nucleon, since O_F is a one-body operator. In contrast the CB matrix element (CBME) can be nonzero even when the occupation numbers of Φ_I and Φ_F differ by more than one nucleon. However, here we consider only the dominant ''one-body'' CBME in which they differ by only one nucleon. We define the quenching factor η as the ratio of the square of these matrix elements, $|\mathrm{CBME}|^2/|\mathrm{FGME}|^2$.

We assume that $|\Phi_I\rangle$ has full neutron and proton Fermi spheres with momenta k_{Fn} and k_{Fp}, and

$$|\Phi_F\rangle=a^\dagger_{\mathbf{k}_p\chi_p}a_{\mathbf{k}_n\chi_n}|\Phi_I\rangle, \tag{13}$$

where $k_n\leqslant k_{Fn}$ and $k_p>k_{Fp}$. In the absence of spin-orbit correlations, the Fermi matrix elements are nonzero only when the spin state $\chi_n=\chi_p$. The FGME$=1$ when $\mathbf{k}_p-\mathbf{k}_n=\mathbf{q}$. These conditions are also necessary for the CBME to be nonzero; however, its value can depend on the matter density, proton fraction, and the magnitudes k_n, k_p, and q.

The cluster expansion of the CBME is obtained by replacing the correlation operators F_{ij} by $1+(F_{ij}-1)$ [31] and expanding the numerator and the denominator in powers of $(F_{ij}-1)$. It is convenient to use the Φ_I^P, containing only a product of single-particle wave functions in which nucleons i are in plane wave states with momentum $\mathbf{k}_i$ and spin-isospin $\chi_\tau(i)$, in place of the antisymmetric Φ_I and use the antisymmetric Φ_F. This is equivalent to retaining the antisymmetric Φ_I and Φ_F and has the advantage that we can associate nucleon numbers with the state labels in Φ_I^P. The nucleon in the state $\mathbf{k}_n\chi_n$ of Φ_I^P is labeled ''a'' for active; in uncorrelated states only a participates in the transition. All other nucleons in the Fermi spheres are denoted by j.

The cluster expansion of the CBME is represented by diagrams as shown in Fig. 1. The terms in the expansion are labeled with $Fnxy$, where F stands for Fermi, n is the order of the $(F_{ij}-1)$ correlations, $x=d,e$ for direct and exchange terms, and $y=a,j$ denoting the nucleon on which the weak

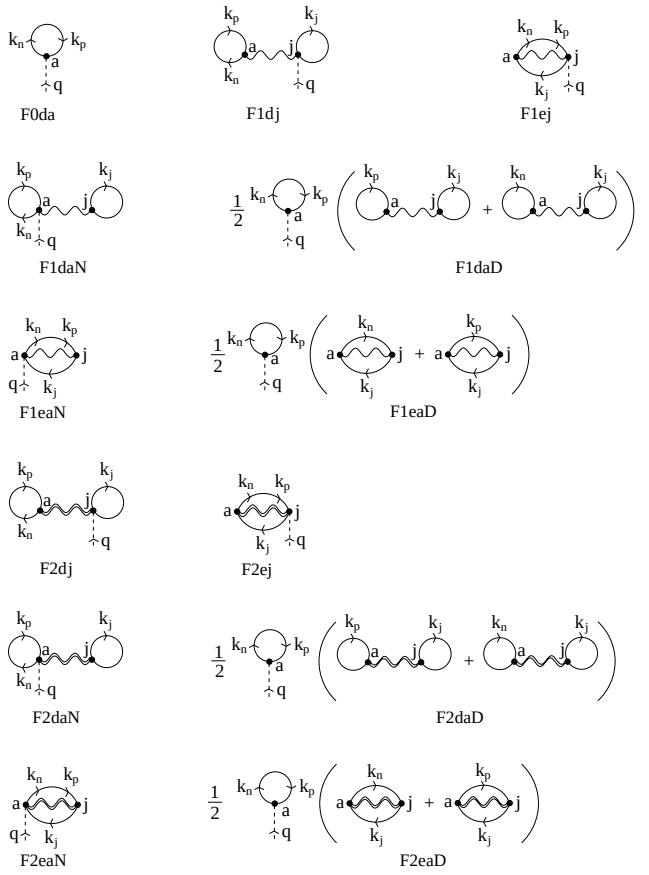

FIG. 1. Diagrams illustrating all of the one- and two-body terms contributing to the Fermi CBME.

interaction operates. The dots in these diagrams denote nucleons, a thin line specifying the states occupied by the nucleon in Φ_I^P and Φ_F passes through each dot. The nucleons a and j occupy states $\mathbf{k}_n$ and $\mathbf{k}_j$ in the Φ_I^P, therefore lines labeled $\mathbf{k}_n$ and $\mathbf{k}_j$ originate from them in all diagrams. Their termination depends on the exchange pattern, since Φ_F is antisymmetric. In direct terms, the state line $\mathbf{k}_j$ emerges and ends in dot j because the state of nucleon j is unchanged. The line with the two labels $\mathbf{k}_n$ and $\mathbf{k}_p$ denotes the weak transition. In direct diagrams it begins and ends in dot a. In diagrams in which a and j are exchanged, the transition line begins at a and ends in j, while the state line $\mathbf{k}_j$ begins from j and ends in a. The state and transition lines must form closed loops in all diagrams. The dashed line attached to nucleon $i=a$ or j shows the Fermi operator $O_F(i) = \boldsymbol{\tau}_i^+ e^{i\mathbf{q}\cdot\mathbf{r}_i}$. The $(F_{ij}-1)$ correlations are indicated by wavy lines. We sum over the spin-isospin states $\chi_\tau(j)$ of the nucleon j, while those of a (χ_n and χ_p), are specified by Φ_F [Eq. (13)].

The equations for $Fnxy$ are given below in the two-body cluster approximation in which $n \leqslant 2$. They show that the $Fnxy$ are independent of q, k_n, and k_p when $x,y=d,a$; they depend only on q when $x,y=d,j$; and only on k_n and k_p in exchange diagrams ($x=e$). We also give a simple explanation of the important $F2da$ term responsible for much of the quenching. The standard second-order perturbation theory calculation of the direct contributions to the Fermi matrix element is reviewed in Appendix A. One can easily identify the analogs of $Fndy$ in that familiar theory and obtain relations between the present approach and that of Arima and coworkers [13]. The perturbation theory assumes that the forces are weak, but in reality we cannot expand in powers of the strong, bare two-nucleon interaction v_{ij}. However, we hope that standard perturbation theory can be used in CB with the effective operators and interactions described here, as mentioned in the Introduction.

The leading zeroth-order term is given by

$$F0da = \mathrm{FGME} = \int d^3r e^{i(\mathbf{k}_n+\mathbf{q}-\mathbf{k}_p)\cdot\mathbf{r}} \langle \chi_p(a)|\boldsymbol{\tau}^+(a)|\chi_n(a)\rangle = 1. \tag{14}$$

The momentum conserving delta function $\delta^3(\mathbf{k}_p-\mathbf{k}_n-\mathbf{q})$ and the $\chi_n=\chi_p$ spin constraint are implied here as well as in all terms of the expansion given below. There are no other zeroth-order terms.

The first-order direct term with $O_F(j\neq a)$ is given by

$$F1dj = \sum_j \int d^3r_{aj} e^{-i\mathbf{q}\cdot\mathbf{r}_{aj}} \times \langle \chi_p(a)\chi_\tau(j)|\{\boldsymbol{\tau}_j^+, (F_{aj}-1)\}|\chi_n(a)\chi_\tau(j)\rangle = \rho \int d^3r e^{-i\mathbf{q}\cdot\mathbf{r}} 2f^\tau(r). \tag{15}$$

All spin dependent terms in F_{aj} give zero contribution on summing over the spin states of nucleons j, and the factor of 2 in the above equation comes from

$$\{\boldsymbol{\tau}_j^+, \boldsymbol{\tau}_j\cdot\boldsymbol{\tau}_a\} = 2\boldsymbol{\tau}_a^+. \tag{16}$$

From now on the aj subscripts on $\mathbf{r}$ and F will be dropped for brevity, and the r dependence of the f^p's will be implicit.

The contribution of $F1ej$ is given by

$$F1ej = \sum_j \int d^3r e^{i(\mathbf{k}_n-\mathbf{k}_j)\cdot\mathbf{r}} \times \langle \chi_p(a)\chi_\tau(j)|e_{aj}\{\boldsymbol{\tau}_j^+, (F-1)\}|\chi_n(a)\chi_\tau(j)\rangle = -\int d^3r e^{i\mathbf{k}_n\cdot\mathbf{r}} [\rho_n \ell_n(r)(f^c-1+3f^\sigma) + \rho_p \ell_p(r)(f^\tau+3f^{\tau\sigma})], \tag{17}$$

where e_{ij} is the spin-isospin exchange operator:

$$e_{ij} = -\frac{1}{4}(1+\boldsymbol{\tau}_i\cdot\boldsymbol{\tau}_j)(1+\boldsymbol{\sigma}_i\cdot\boldsymbol{\sigma}_j), \tag{18}$$

and the Slater functions ($N=n,p$) are

$$\ell_N(r)=\frac{2}{\rho_N}\int\frac{d^3k}{(2\pi)^3}\theta(k_{FN}-k)e^{i\mathbf{k}\cdot\mathbf{r}}=3[\sin(k_{FN}r)-k_{FN}r\cos(k_{FN}r)]/(k_{FN}r)^3. \tag{19}$$

The algebra of the operators $O_{aj}^{p=1,6}$ described in Ref. [31] is very useful in evaluating these contributions.

The two-body terms with $O_F(a)$ have contributions from the numerator of the matrix element, Eq. (12), as well as normalization corrections introduced through the expansion of the denominator. We denote these by $F1xaN$ and $F1xaD$, respectively. In Fig. 1 the denominator contributions are shown as products of two diagrams. The first-order direct terms with $O_F(a)$ cancel:

$$F1da=F1daN+F1daD=0, \tag{20}$$

while for the exchange terms we obtain

$$F1ea=F1eaN+F1eaD \tag{21}$$

$$\begin{aligned}F1eaN&=\sum_j\int d^3re^{-i(\mathbf{k}_j-\mathbf{k}_p)\cdot\mathbf{r}}\langle\chi_p(a)\chi_\tau(j)|\\&\quad\times e_{aj}\{\boldsymbol{\tau}_a^+,(F-1)\}|\chi_n(a)\chi_\tau(j)\rangle\\&=-\int d^3re^{i\mathbf{k}_p\cdot\mathbf{r}}[\rho_p\ell_p(f^c-1+3f^\sigma)\\&\quad+\rho_n\ell_n(f^\tau+3f^{\sigma\tau})],\end{aligned} \tag{22}$$

$$\begin{aligned}F1eaD&=\sum_j-\int d^3r[e^{-i(\mathbf{k}_j-\mathbf{k}_n)\cdot\mathbf{r}}\langle\chi_n(a)\chi_\tau(j)|\\&\quad\times e_{aj}(F-1)|\chi_n(a)\chi_\tau(j)\rangle\\&\quad+e^{-i(\mathbf{k}_j-\mathbf{k}_p)\cdot\mathbf{r}}\langle\chi_p(a)\chi_\tau(j)|\\&\quad\times e_{aj}(F-1)|\chi_p(a)\chi_\tau(j)\rangle]\\&=\frac{1}{2}\int d^3r([f^c-1+3f^\sigma+f^\tau+3f^{\sigma\tau}]\\&\quad\times[e^{i\mathbf{k}_n\cdot\mathbf{r}}\rho_n\ell_n+e^{i\mathbf{k}_p\cdot\mathbf{r}}\rho_p\ell_p]+2[f^\tau+3f^{\sigma\tau}]\\&\quad\times[e^{i\mathbf{k}_n\cdot\mathbf{r}}\rho_p\ell_p+e^{i\mathbf{k}_p\cdot\mathbf{r}}\rho_n\ell_n]).\end{aligned} \tag{23}$$

For calculating the second-order terms, it is convenient to define

$$F=1+F^0+F^1\boldsymbol{\tau}_a\cdot\boldsymbol{\tau}_j, \tag{24}$$

$$F^0=f^c-1+f^\sigma\boldsymbol{\sigma}_a\cdot\boldsymbol{\sigma}_j+f^tS_{aj}, \tag{25}$$

$$F^1=f^\tau+f^{\sigma\tau}\boldsymbol{\sigma}_a\cdot\boldsymbol{\sigma}_j+f^{t\tau}S_{aj}. \tag{26}$$

Only the spin independent parts of the products of the above F^0 and F^1 contribute to the second-order diagrams. These are called the C parts in Ref. [31]. We define

$$C_d^{IJ}=C[F^IF^J], \tag{27}$$

$$C_e^{IJ}=C[(1+\boldsymbol{\sigma}_a\cdot\boldsymbol{\sigma}_j)F^IF^J]. \tag{28}$$

The expressions for C_d^{IJ} and C_e^{IJ} in terms of the correlation functions f^p are given in Appendix B.

There is no contribution from the denominator to the terms $F2xj$. These are given by

$$\begin{aligned}F2dj&=\sum_j\int d^3re^{-i\mathbf{q}\cdot\mathbf{r}}\langle\chi_p(a)\chi_\tau(j)|\\&\quad\times(F-1)\boldsymbol{\tau}_j^+(F-1)|\chi_n(a)\chi_\tau(j)\rangle\\&=\rho\int d^3re^{-i\mathbf{q}\cdot\mathbf{r}}\,2[C_d^{11}+C_d^{01}],\end{aligned} \tag{29}$$

$$\begin{aligned}F2ej&=\sum_j\int d^3re^{i(\mathbf{k}_n-\mathbf{k}_j)\cdot\mathbf{r}}\langle\chi_p(a)\chi_\tau(j)|\\&\quad\times e_{aj}(F-1)\boldsymbol{\tau}_j^+(F-1)|\chi_n(a)\chi_\tau(j)\rangle\\&=-\frac{1}{2}\int d^3re^{i\mathbf{k}_n\cdot\mathbf{r}}[\rho_n\ell_n(C_e^{00}-C_e^{11})\\&\quad+2\rho_p\ell_p(C_e^{11}+C_e^{01})].\end{aligned} \tag{30}$$

The sum

$$\begin{aligned}F2da&=F2daN+F2daD\\&=\sum_j\int d^3r\langle\chi_p(a)\chi_\tau(j)|(F-1)\boldsymbol{\tau}_a^+(F-1)\\&\quad-\frac{1}{2}\{\boldsymbol{\tau}_a^+,(F-1)^2\}|\chi_n(a)\chi_\tau(j)\rangle\\&=\rho\int d^3r(-4C_d^{11}).\end{aligned} \tag{31}$$

Note that only the $F^1\boldsymbol{\tau}_a\cdot\boldsymbol{\tau}_j$, which does not commute with the $\boldsymbol{\tau}_a^+$ operator, contributes to this sum.

The results presented in the following section show that the above term gives the largest contribution to the quenching of the Fermi matrix element in matter. This term simply takes into account the probability for nucleon a to be a neutron in the initial and a proton in the final state. In the uncorrelated product state $|\Phi_I^P\rangle$, nucleon a is $n\uparrow$; but in the correlated product state $\mathcal{S}\Pi F_{ij}|\Phi_I^P\rangle$, it can be in other nucleon states. We refer to nucleon a in the correlated state as a ''quasinucleon.'' The probability that it is a neutron is given by

$$P_I(a=n)=\frac{\langle\Phi_I|[\mathcal{S}\Pi F_{ij}]\frac{1}{2}(1-\tau_a^z)[\mathcal{S}\Pi F_{ij}]|\Phi_I^P\rangle}{\langle\Phi_I|[\mathcal{S}\Pi F_{ij}]^2|\Phi_I^P\rangle}. \tag{32}$$

We use the cluster expansion to calculate this probability. The zeroth-order, one-body term is unit, and the two-body second-order direct term is

TABLE I. Correlated basis probabilities for the active quasinucleon a to be $N\uparrow$ and $N\downarrow$ in the initial state for $\rho=(\frac{1}{2},\ 1,\ \frac{3}{2})\rho_0$ and $x_p=0.5$. The listed values include contributions of one- and two-body direct terms.

I	$P(a,\frac{1}{2}\rho_0)$	$P(a,\rho_0)$	$P(a,\frac{3}{2}\rho_0)$
$n\uparrow$	0.92	0.89	0.87
$n\downarrow$	0.02	0.03	0.03
$p\uparrow$	0.02	0.03	0.03
$p\downarrow$	0.04	0.05	0.07

$$-\frac{1}{2}\sum_j \int d^3r\langle\chi_n(a)\chi_\tau(j)|(F-1)\tau_a^z(F-1)$$
$$-\frac{1}{2}\{\tau_a^z,(F-1)^2\}|\chi_n(a)\chi_\tau(j)\rangle$$
$$=\rho_p\int d^3r(-4C_d^{11}). \tag{33}$$

The two-body first-order direct terms cancel as in Eq. (20). Neglecting the exchange terms, we obtain the direct part

$$P_I(a=n,d)=1+\rho_p\int d^3r(-4C_d^{11}). \tag{34}$$

In a similar way, the direct part of the probability for the active quasinucleon a to be a proton in the final state is given by

$$P_F(a=p,d)=1+\rho_n\int d^3r(-4C_d^{11}). \tag{35}$$

Hence

$$1+F2da=P_I(a=n,d)P_F(a=p,d), \tag{36}$$

neglecting the terms of order $(C_d^{11})^2$.

The probabilities for the active quasinucleon to be in the initial spin isospin states $\uparrow,\downarrow n,p$ have been calculated keeping only the direct terms, at the three densities for $x_p=0.5$. These are given in Table I. In one-body Fermi transitions these are also the probabilities for the active quasinucleon to be a spin $\uparrow,\downarrow p,n$ in the final state.

The second-order exchange term

$$F2ea=F2eaN+F2eaD \tag{37}$$

has contributions from both F^1 and F^0. They are given by

$$F2eaN=\sum_j \int d^3re^{i(\mathbf{k}_p-\mathbf{k}_j)\cdot\mathbf{r}}\langle\chi_p(a)\chi_\tau(j)|$$
$$\times e_{aj}(F-1)\boldsymbol{\tau}_a^+(F-1)|\chi_n(a)\chi_\tau(j)\rangle$$
$$=-\frac{1}{2}\int d^3re^{i\mathbf{k}_p\cdot\mathbf{r}}[\rho_p\ell_p(C_e^{00}-C_e^{11})$$
$$+2\rho_n\ell_n(C_e^{11}+C_e^{10})], \tag{38}$$

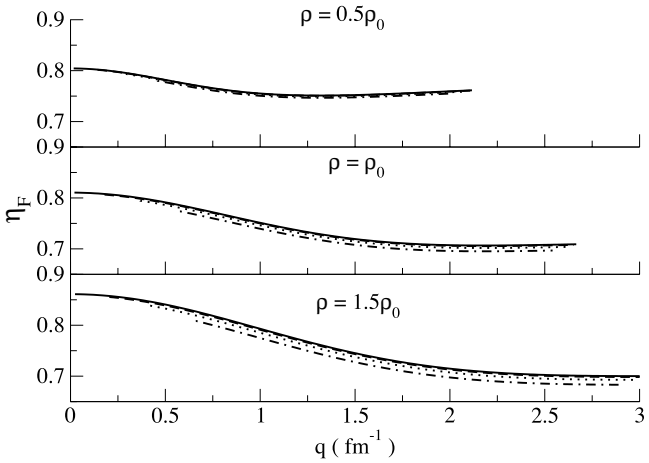

FIG. 2. η_F as a function of q and proton fraction x_p for $k_N=k_{FN}$. The solid, dashed, dotted, and dash-dot lines show results for $x_p=0.5$, 0.4, 0.3, and 0.2.

$$F2eaD=\sum_j -\frac{1}{2}\int d^3r[e^{-i(\mathbf{k}_j-\mathbf{k}_n)\cdot\mathbf{r}}\langle\chi_n(a)\chi_\tau(j)|$$
$$\times e_{aj}(F-1)^2|\chi_n(a)\chi_\tau(j)\rangle+e^{-i(\mathbf{k}_j-\mathbf{k}_p)\cdot\mathbf{r}}$$
$$\times\langle\chi_p(a)\chi_\tau(j)|e_{aj}(F-1)^2|\chi_p(a)\chi_\tau(j)\rangle]$$
$$=\frac{1}{4}\int d^3r[(-4C_e^{11}+4C_e^{10})(e^{i\mathbf{k}_n\cdot\mathbf{r}}\rho_p\ell_p$$
$$+e^{i\mathbf{k}_p\cdot\mathbf{r}}\rho_n\ell_n)+(C_e^{00}+C_e^{11}+2C_e^{10})(e^{i\mathbf{k}_n\cdot\mathbf{r}}\rho_n\ell_n$$
$$+e^{i\mathbf{k}_p\cdot\mathbf{r}}\rho_p\ell_p)]. \tag{39}$$

Results for Fermi matrix element

The Fermi matrix elements have been calculated using correlation functions obtained in Ref. [9] by minimizing the energy of symmetric nuclear matter using the Argonne-v18 and Urbana-IX two- and three-nucleon interactions. In Fig. 2 we present the results for η_F, the square of the Fermi CBME [Eq. (12)], for $k_n=k_{Fn}$ and $k_p=k_{Fp}$.

When $x_p<0.5$ the total isospin T_I of the state $|I\rangle$ is $(N-Z)/2$, while that of $|F\rangle$ is $(N-Z)/2-1$. In the case of symmetric nuclear matter the $T_I=0$, while $T_F=1$. Thus the calculated matrix elements are between states with $\Delta T=1$. The Fermi matrix elements for $q=0$, between isobaric analog states having the same T and $T_{zF}=T_{zI}\pm1$, are given by $(T\mp T_{zI})(T\pm T_{zI}+1)$ in both correlated and uncorrelated states. We will not discuss $\Delta T=0$ Fermi ME in this paper.

The variation of η_F with proton fraction is less than 3% at all densities calculated. However, the proton fraction limits the allowed values of q through the momentum conservation relation: $\mathbf{q}=\mathbf{k}_p-\mathbf{k}_n$. The variation with total density is also small within the considered range. This suggests that we can approximate $|\mathrm{CBME}|^2$ by a function of ρ and q. In the small q region, $q\lesssim0.5$ fm^{-1}, it can be well represented by the quadratic

$$\eta_F=\eta_F(q\to0)+\alpha_F(\rho)q^2. \tag{40}$$

TABLE II. Quadratic fit to η_F and η_{GT} at small q.

ρ	$\lvert\langle O_F\rangle\rvert^2(q=0)$	α_F	$\eta_{GT}(q=0)$	α_{GT}
0.08	0.80	−0.094	0.76	0.259
0.16	0.81	−0.075	0.75	0.060
0.24	0.86	−0.083	0.78	0.041

We have fit the calculated values for symmetric nuclear matter and the results are given in Table II.

Figure 3 shows the contributions of each term in the cluster expansion of the Fermi matrix element in matter at density ρ_0 and $x_p=0.5$. The $Fnxa$ and $Fnej$ terms give contributions that are independent of **q** as can be seen from Eqs. (17), (22), (23), (30), (31), (38), and (39). The dominant contribution to the quenching of the Fermi CBME comes from $F2da$; $|1+F2da|^2=0.7$ is shown by the dotted line in Fig. 3. As discussed in the preceding section this result can be interpreted in terms of the probabilities for the active quasinucleon a to be a neutron in the initial and a proton in the final CB states.

The exchange terms $Fnea$, contribute an additional ~ 0.1 to the q-independent quenching; $|\Sigma_{n,x}Fnxa|^2=0.61$ is shown by the double-dash-dot line. This additional quenching is mostly canceled by the $Fnej$ terms, as shown by the dash-double-dot line; $|\Sigma_{n,x}Fnxa+Fnej|^2=0.71$.

The $Fndj$ terms, given by Eqs. (15) and (29), introduce the q dependence. Of these, the second-order $F2dj$ is dominant as can be seen from the dashed line, which includes only $F1dj$ and all the q-independent terms. The full line gives the square of the total matrix element including $F2dj$.

The contributions of the various correlations to the CBME are shown in Fig. 4. The first- and second-order terms are dominated by the $f^{\sigma\tau}(r_{ij})\boldsymbol{\sigma}_i\cdot\boldsymbol{\sigma}_j\boldsymbol{\tau}_i\cdot\boldsymbol{\tau}_j$ and $f^{t\tau}(r_{ij})S_{ij}\boldsymbol{\tau}_i\cdot\boldsymbol{\tau}_j$ correlations induced mainly by the one pion exchange potential (OPEP). After setting $f^{\sigma\tau}=f^{t\tau}=0$, the $|\Sigma_{n,x}Fnxa|^2$ becomes essentially 1 as shown by the dotted line in Fig. 4. The full CBME exceeds unity in this case (see the dashed line)

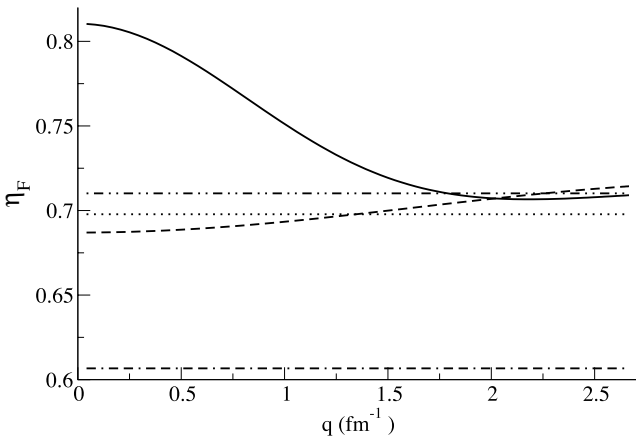

FIG. 3. Contributions to η_F for $k_N=k_{FN}$ and $\rho=\rho_0$. The dash-double dot line includes all of the q-independent terms, while the solid line shows the full result. See text for description of other curves.

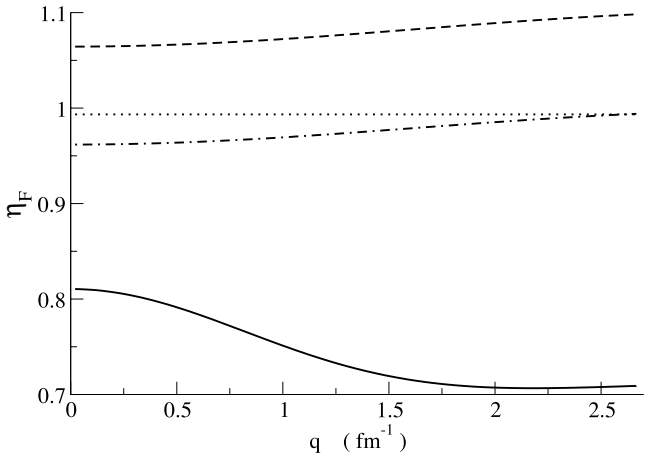

FIG. 4. Correlation dependence of η_F for $k_N=k_{FN}$ and $\rho=\rho_0$. The dashed line shows results with $f^{\sigma\tau}=f^{t\tau}=0$, and in addition, $f^c=1$ for the dash-dot line. The dotted line shows $|\Sigma_{n,x}Fnxa|^2$ when $f^{\sigma\tau}=f^{t\tau}=0$. The solid line gives the full result.

via the contributions of f^c-1 correlations to $Fnxj$. The dash-dot line shows η_F obtained by further setting $f^c=1$. It is fairly close to one showing that the f^τ, f^σ, and f^t correlations have small effects.

The Fermi CBME calculated in the two-body cluster approximation does not depend significantly on the magnitudes of the initial and final nucleon momenta. The dependence on $k_{Fn}-k_n$ and k_p-k_{Fp} is illustrated in Fig. 5. It shows η_F for $\rho=\rho_0$, $x_p=0.5$ and 0.3, $k_n=(1,0.75,0.5)k_{Fn}$, and $k_p=(1,1.25,1.5)k_{Fp}$ as a function of q. The results for the 18 possible combinations of x_p, k_n, and k_p values differ by less than 0.03.

III. CORRELATED BASIS GAMOW-TELLER MATRIX ELEMENT

The procedure for the calculation of the GT matrix element is similar to that discussed in Sec. II. We therefore discuss only the differences and give the final expressions.

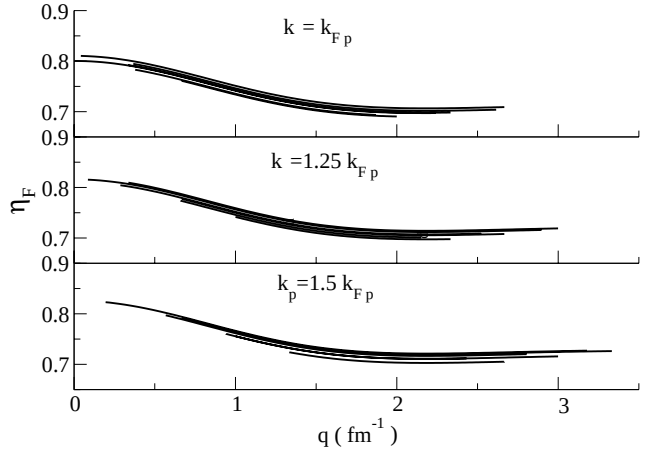

FIG. 5. Dependence of η_F on the initial (k_n) and final (k_p) momenta for $\rho=\rho_0$. Each set contains six lines depicting the results for $k_n=(0.5,0.75,1)k_{Fn}$, and $x_p=0.3$ and 0.5 for the indicated value of k_p.

The operator $\mathbf{O}_{GT}$ is an axial vector and it is convenient to express its matrix element using the following two axial vectors:

$$\langle\widetilde{\boldsymbol{\sigma}_a}\rangle=\langle\chi_p(a)|\boldsymbol{\sigma}(a)\boldsymbol{\tau}^+(a)|\chi_n(a)\rangle \tag{41}$$

and

$$\langle\widetilde{\mathbf{A}_t}\rangle=3\hat{\mathbf{r}}_{aj}\langle\widetilde{\boldsymbol{\sigma}_a}\rangle\cdot\hat{\mathbf{r}}_{aj}-\langle\widetilde{\boldsymbol{\sigma}_a}\rangle, \tag{42}$$

obtained from the tensor correlations between nucleons a and j. Note that $\langle\widetilde{\mathbf{A}_t}\rangle$ depends on $\hat{\mathbf{r}}_{aj}$.

We assume that χ_n in Eq. (13) is spin-up and sum the square of the GT matrix element for the two final states with $\chi_p=\uparrow,\downarrow$ denoted by $|F\uparrow\rangle$ and $|F\downarrow\rangle$. In FG we get contributions only via the operator $\widetilde{\boldsymbol{\sigma}_a}=\boldsymbol{\sigma}_a\boldsymbol{\tau}_a^+$; only $\sigma_z(a)$ contributes to the FGME with $\chi_p=\uparrow$, while $\sigma_x(a)$ and $\sigma_y(a)$ give the GT FGME for $\chi_p=\downarrow$. However, in CB the $\widetilde{\mathbf{A}_t}$ induces transitions that are forbidden in FG states.

The terms in the cluster expansion of the GT CBME are denoted by GTnxy as in the last section. The ratio g_A of the axial to vector coupling constants is omitted from the GTnxy for brevity. We obtain

$$\mathrm{GT0}da=\langle\widetilde{\boldsymbol{\sigma}_a}\rangle, \tag{43}$$

$$\mathrm{GT1}dj=\rho\int d^3r e^{-i\mathbf{q}\cdot\mathbf{r}}2(f^{\sigma\tau}\langle\widetilde{\boldsymbol{\sigma}_a}\rangle+f^{t\tau}\langle\widetilde{\mathbf{A}_t}\rangle), \tag{44}$$

$$\begin{aligned}\mathrm{GT1}ej=-\int d^3r e^{i\mathbf{k}_n\cdot\mathbf{r}}\{&\rho_p\ell_p(f^\tau+3f^{\sigma\tau})\langle\widetilde{\boldsymbol{\sigma}_a}\rangle+\rho_n\ell_n[(f^c-1\\&+f^\sigma+2f^{\sigma\tau})\langle\widetilde{\boldsymbol{\sigma}_a}\rangle+(f^t-f^{t\tau})\langle\widetilde{\mathbf{A}_t}\rangle]\},\end{aligned} \tag{45}$$

$$\begin{aligned}\mathrm{GT1}eaN=-\int d^3r e^{i\mathbf{k}_p\cdot\mathbf{r}}\{&\rho_n\ell_n(f^\tau+3f^{\sigma\tau})\langle\widetilde{\boldsymbol{\sigma}_a}\rangle+\rho_p\ell_p[(f^c\\&-1+f^\sigma+2f^{\sigma\tau})\langle\widetilde{\boldsymbol{\sigma}_a}\rangle+(f^t-f^{t\tau})\langle\widetilde{\mathbf{A}_t}\rangle]\},\end{aligned} \tag{46}$$

$$\mathrm{GT1}eaD=\langle\widetilde{\boldsymbol{\sigma}_a}\rangle F1eaD, \tag{47}$$

$$\begin{aligned}\mathrm{GT2}dj=2\rho\int d^3r e^{-i\mathbf{q}\cdot\mathbf{r}}[&(F_{d,j}^{11,\sigma}+F_{d,j}^{01,\sigma})\langle\widetilde{\boldsymbol{\sigma}_a}\rangle+(F_{d,j}^{11,A}\\&+F_{d,j}^{01,A})\langle\widetilde{\mathbf{A}_t}\rangle],\end{aligned} \tag{48}$$

$$\begin{aligned}\mathrm{GT2}ej=-\frac{1}{2}\int d^3r e^{i\mathbf{k}_n\cdot\mathbf{r}}\{&\rho_n\ell_n[(F_{e,j}^{00,\sigma}-F_{e,j}^{11,\sigma}-F_{e,j}^{10,\sigma}\\&+F_{e,j}^{01,\sigma})\langle\widetilde{\boldsymbol{\sigma}_a}\rangle+(F_{e,j}^{00,A}-F_{e,j}^{11,A}-F_{e,j}^{10,A}+F_{e,j}^{01,A})\langle\widetilde{\mathbf{A}_t}\rangle]\\&+2\rho_p\ell_p[(F_{e,j}^{11,\sigma}+F_{e,j}^{01,\sigma})\langle\widetilde{\boldsymbol{\sigma}_a}\rangle\\&+(F_{e,j}^{11,A}+F_{e,j}^{01,A})\langle\widetilde{\mathbf{A}_t}\rangle]\},\end{aligned} \tag{49}$$

$$\mathrm{GT2}da=\rho\int d^3r(F_{d,a}^{00,\sigma}-F_{d,a}^{11,\sigma}-C_d^{00}-3C_d^{11})\langle\widetilde{\boldsymbol{\sigma}_a}\rangle, \tag{50}$$

$$\begin{aligned}\mathrm{GT2}eaN=-\frac{1}{2}\int d^3r e^{i\mathbf{k}_p\cdot\mathbf{r}}\{&\rho_p\ell_p[(F_{e,a}^{00,\sigma}-F_{e,a}^{11,\sigma}+F_{e,a}^{10,\sigma}\\&-F_{e,a}^{01,\sigma})\langle\widetilde{\boldsymbol{\sigma}_a}\rangle+(F_{e,a}^{00,A}-F_{e,a}^{11,A}+F_{e,a}^{10,A}\\&-F_{e,a}^{01,A})\langle\widetilde{\mathbf{A}_t}\rangle]+2\rho_n\ell_n[(F_{e,a}^{11,\sigma}+F_{e,a}^{10,\sigma})\langle\widetilde{\boldsymbol{\sigma}_a}\rangle\\&+(F_{e,a}^{11,A}+F_{e,a}^{10,A})\langle\widetilde{\mathbf{A}_t}\rangle]\},\end{aligned} \tag{51}$$

$$\mathrm{GT2}eaD=\langle\widetilde{\boldsymbol{\sigma}_a}\rangle F2eaD. \tag{52}$$

The coefficients $F_{d,y}^{IJ,\sigma}$ $(y=a,j)$ and $F_{d,y}^{IJ,A}$ are defined as the $\boldsymbol{\sigma}_a$ and $\mathbf{A}_t$ parts of the operator $F^I\boldsymbol{\sigma}_yF^J$:

$$F^I\boldsymbol{\sigma}_yF^J=F_{d,y}^{IJ,\sigma}\boldsymbol{\sigma}_a+F_{d,y}^{IJ,A}\mathbf{A}_t+(\text{terms linear in }\boldsymbol{\sigma}_j). \tag{53}$$

The remaining parts linear in $\boldsymbol{\sigma}_j$ do not contribute after summing over $\boldsymbol{\sigma}_j$. The $F_{e,y}^{IJ,\sigma}$ and $F_{e,y}^{IJ,A}$ are the corresponding parts of the operator $(1+\boldsymbol{\sigma}_a\cdot\boldsymbol{\sigma}_j)F^I\boldsymbol{\sigma}_yF^J$, and the expressions for $F_{x,y}^{IJ,\sigma}$ and $F_{x,y}^{IJ,A}$ are given in Appendix B.

As in the Fermi case, the second-order direct diagrams, GT2da can be interpreted in terms of quasinucleon probabilities. The GT2da has contributions from $\langle\widetilde{\boldsymbol{\sigma}_a}\rangle$ only. When the final proton has spin $\uparrow$ only the σ_a^z term contributes. We consider this simple case for illustration. In this case, $(1+\mathrm{GT2}da)$ represents the probability that the active quasinucleon has $\sigma_a^z\tau_a^z=-1$ in the initial state and $+1$ in the final state. In FG states these are unit probabilities. We use the cluster expansion to calculate them in CB states. The zeroth-order terms are equal to 1, and the two-body second-order direct terms are given by

$$\begin{aligned}\mp\frac{1}{2}\sum_j\int d^3r\langle\chi_n(a)\chi_\tau(j)|&(F-1)\sigma_a^z\tau_a^z(F-1)\\&-\frac{1}{2}\{\sigma_a^z\tau_a^z,\,(F-1)^2\}|\chi_n(a)\chi_\tau(j)\rangle\\=\rho\frac{1}{2}\int d^3r&(F_{d,a}^{00,\sigma}-F_{d,a}^{11,\sigma}-C_d^{00}\\&-3C_d^{11})\mp(\rho_p-\rho_n)\frac{1}{2}\int d^3r(F_{d,a}^{10,\sigma}+F_{d,a}^{01,\sigma}+2F_{d,a}^{11,\sigma}\\&-2C_d^{10}+2C_d^{11}),\end{aligned} \tag{54}$$

where the upper and lower signs correspond to the initial and final states, respectively. The first-order direct terms cancel as in Eq. (20). Neglecting the exchange terms and those of order $C_d^{IJ}C_d^{MN}$ and $F_{d,a}^{IJ,\sigma}F_{d,a}^{MN,\sigma}$ we obtain

$$\begin{aligned}P_I(\sigma_a^z\tau_a^z=-1,d)P_F(\sigma_a^z\tau_a^z=1,d)&\\=1+\rho\int d^3r(F_{d,a}^{00,\sigma}-F_{d,a}^{11,\sigma}-C_d^{00}-3C_d^{11})&\\=1+[\mathrm{GT2}da]_z.&\end{aligned} \tag{55}$$

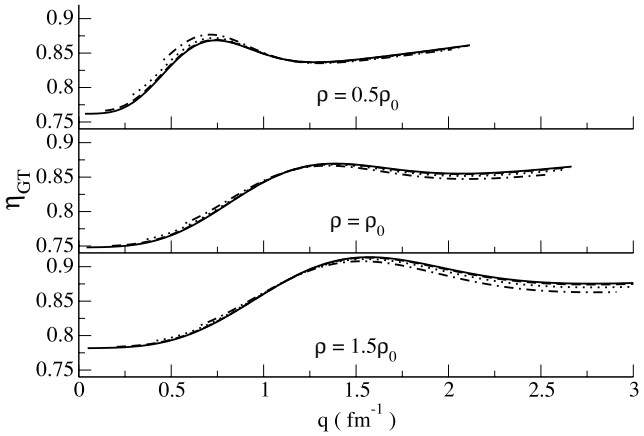

FIG. 6. η_{GT} as a function of q and proton fraction x_p for $k_N = k_{FN}$. The solid, dashed, dotted, and dash-dot lines show results for $x_p = 0.5$, 0.4, 0.3, and 0.2.

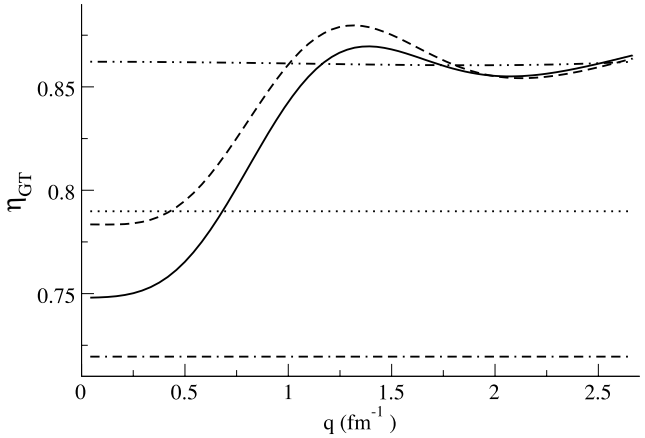

FIG. 7. Contributions to the η_{GT} for for $k_N = k_{FN}$ and $\rho = \rho_0$: the dash-double dot line includes all of the q-independent terms, while the solid line shows the full result. See text for description of other curves.

The $\sigma_a^z \tau_a^z = -1$ probability is the sum of the $n\uparrow$ and $p\downarrow$ probabilities listed in Table I.

Results of Gamow-Teller matrix element

The tensor correlations lead to a dependence of the GT CBME on the direction of the spin quantization axis through the $\langle \widetilde{\mathbf{A}_t} \rangle$ terms. We therefore do not discuss the CBME for spin-up and -down final states individually. The sum of $|\mathrm{CBME}|^2$ over the final two spin states determines the transition rates and is independent of the chosen axis. This sum equals 3 for FGME. In the following, we report results for

$$\eta_{GT} \equiv \tfrac{1}{3}(|\langle F\uparrow|\mathbf{O}_{GT}|I\rangle|^2 + |\langle F\downarrow|\mathbf{O}_{GT}|I\rangle|^2). \qquad (56)$$

The η_{GT} has been calculated using the correlation functions as described in Sec. II and the results for $k_N = k_{FN}$ are plotted in Fig. 6. As in the Fermi case, the variation of η_{GT} due to changes in proton fraction is less than 3%, but it has more q dependence. The quadratic fit [Eq. (40)] is still valid up to $q \sim 0.5$ fm^{-1}, and its parameters are given in Table II.

Figure 7 illustrates the relative contributions of the various terms to η_{GT}. As in the Fermi case, the main quenching comes from the GT2da term; approximating the $|\mathrm{CBME}|^2$ by $|1 + \mathrm{GT2}da|^2$ gives $\eta_{GT} = 0.79$ (dotted line). It decreases to 0.72 on adding the GTnea terms (double-dash-dot line). The double-dot-dash line shows the result after including GTnej terms that reduce the quenching.

The main q dependence comes from the first-order GT1dj term; results obtained after adding this term are shown by the dashed line. The GT2dj term also contributes to the q dependence (full line gives the total η_{GT}).

The dash-dot and the double-dot-dash lines have a barely visible q dependence coming from the GTney terms. In the Fermi case these exchange terms depend only on k_n and k_p; however, in the GT case they introduce a dependence of η_{GT} on the angle between $\mathbf{k}_n$ and $\mathbf{k}_p$. This appears as a q dependence, but it is very small (<0.002).

The relative contributions of various correlations to η_{GT} are shown in Fig. 8. The dashed and the dash-dot lines show results obtained after setting $f^{\sigma\tau} = f^{t\tau} = 0$, and in addition $f^c = 1$, respectively. The central correlations contribute mostly via the GTnej terms; the dotted line close to $\eta_{GT} = 1$ is obtained by setting $f^{\sigma\tau} = f^{t\tau} = 0$ and including only the GTnxa terms.

The dependence of η_{GT} on k_n and k_p is shown in Fig. 9. It is small <0.03 as for η_F.

IV. CORRELATED BASIS NEUTRAL-VECTOR MATRIX ELEMENT

In ''one-body'' NV transitions the final state is

$$|\Phi_F\rangle = a^\dagger_{\mathbf{k}_f \chi_N^f} a_{\mathbf{k}_i \chi_N^i} |\Phi_I\rangle, \qquad (57)$$

where $k_i \leq k_{FN}$ and $k_f > k_{FN}$. The NV matrix element is nonzero only when the initial and final spin-isospin states χ_N^f and χ_N^i are the same.

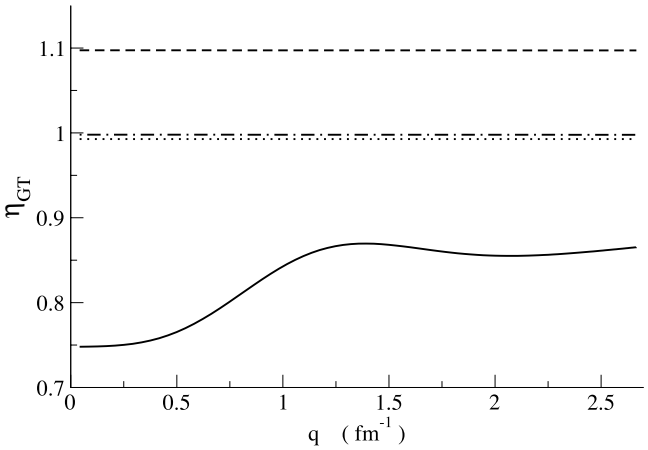

FIG. 8. Correlation dependence of η_{GT} for $k_N = k_{FN}$ and $\rho = \rho_0$. The solid line is for η_{GT} with the full F. The dashed line shows results with $f^{\sigma\tau} = f^{t\tau} = 0$, and in addition, $f^c = 1$ for the dash-dot line. The dotted line shows $\overline{|\Sigma_{n,x}\mathrm{GT}nxa|^2}$ when $f^{\sigma\tau} = f^{t\tau} = 0$.

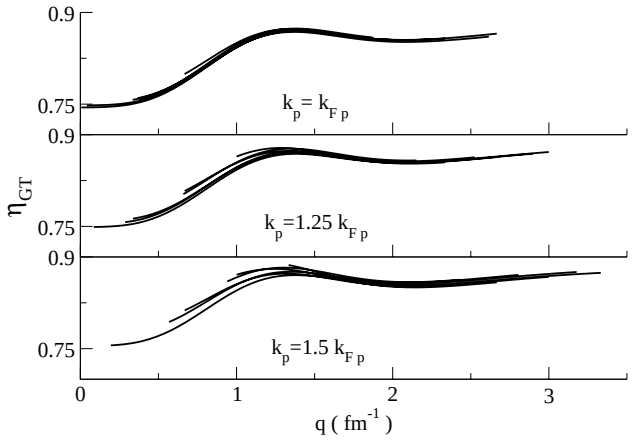

FIG. 9. Dependence of the η_{GT} on the initial (k_n) and final (k_p) momenta for $\rho=\rho_0$. Each set contains six lines depicting the results for $k_n=(0.5,0.75,1)k_{Fn}$, and $x_p=0.3$ and 0.5 for the indicated value of k_p.

The terms in the cluster expansion of the NV CBME are denoted by

$$\mathrm{NV}nxy = -\sin^2\theta_W \mathrm{NV}nxy1 + \tfrac{1}{2}(1-2\sin^2\theta_W)\mathrm{NV}nxyz, \tag{58}$$

where n, x, and y are defined in Sec. II and 1 and z, respectively, represent contributions of $e^{i\mathbf{q}\cdot\mathbf{r}_i}$ and $\tau_i^z e^{i\mathbf{q}\cdot\mathbf{r}_i}$. For the NV$nxy1$ terms we obtain

$$\mathrm{NV0}da1 = 1, \tag{59}$$

$$\mathrm{NV1}dj1 = \int d^3r e^{-i\mathbf{q}\cdot\mathbf{r}} 2[(f^c-1)\rho + f^\tau(\rho_p-\rho_n)\langle\tau_a^z\rangle], \tag{60}$$

$$\mathrm{NV1}ej1 = -\frac{1}{2}\int d^3r e^{i\mathbf{k}_i\cdot\mathbf{r}}\{(f^c-1+3f^\sigma+3f^\tau+9f^{\sigma\tau})(\rho_p\ell_p + \rho_n\ell_n) + (f^c-1+3f^\sigma-f^\tau-3f^{\sigma\tau})(\rho_p\ell_p-\rho_n\ell_n) \times\langle\tau_a^z\rangle\}, \tag{61}$$

$$\mathrm{NV1}da1 = 0, \tag{62}$$

$$\mathrm{NV1}eaN1 = -\frac{1}{2}\int d^3r e^{i\mathbf{k}_f\cdot\mathbf{r}}\{(f^c-1+3f^\sigma+3f^\tau+9f^{\sigma\tau}) \times(\rho_p\ell_p+\rho_n\ell_n) + (f^c-1+3f^\sigma-f^\tau-3f^{\sigma\tau}) \times(\rho_p\ell_p-\rho_n\ell_n)\langle\tau_a^z\rangle\}, \tag{63}$$

$$\mathrm{NV1}eaD1 = \frac{1}{4}\int d^3r (e^{i\mathbf{k}_i\cdot\mathbf{r}}+e^{i\mathbf{k}_f\cdot\mathbf{r}})[(f^c-1+3f^\sigma+3f^\tau +9f^{\sigma\tau})(\rho_p\ell_p+\rho_n\ell_n) + (f^c-1+3f^\sigma-f^\tau -3f^{\sigma\tau})(\rho_p\ell_p-\rho_n\ell_n)\langle\tau_a^z\rangle], \tag{64}$$

$$\mathrm{NV2}dj1 = \int d^3r e^{-i\mathbf{q}\cdot\mathbf{r}}[(C_d^{00}+3C_d^{11})\rho + 2(C_d^{10}-C_d^{11})(\rho_p-\rho_n)\langle\tau_a^z\rangle], \tag{65}$$

$$\mathrm{NV2}ej1 = -\frac{1}{4}\int d^3r e^{i\mathbf{k}_i\cdot\mathbf{r}}\{(C_e^{00}+6C_e^{10}-3C_e^{11})(\rho_p\ell_p + \rho_n\ell_n) + (C_e^{00}-2C_e^{10}+5C_e^{11})(\rho_p\ell_p-\rho_n\ell_n) \times\langle\tau_a^z\rangle\}, \tag{66}$$

$$NV2da1 = 0, \tag{67}$$

$$\mathrm{NV2}eaN1 = -\frac{1}{4}\int d^3r e^{i\mathbf{k}_f\cdot\mathbf{r}}\{(C_e^{00}+6C_e^{10}-3C_e^{11}) \times(\rho_p\ell_p+\rho_n\ell_n) + (C_e^{00}-2C_e^{10}+5C_e^{11}) \times(\rho_p\ell_p-\rho_n\ell_n)\langle\tau_a^z\rangle\}, \tag{68}$$

$$\mathrm{NV2}eaD1 = \frac{1}{8}\int d^3r (e^{i\mathbf{k}_i\cdot\mathbf{r}}+e^{i\mathbf{k}_f\cdot\mathbf{r}})[(C_e^{00}+6C_e^{01}-3C_e^{11}) \times(\rho_p\ell_p+\rho_n\ell_n) + (C_e^{00}-2C_e^{01}+5C_e^{11})(\rho_p\ell_p - \rho_n\ell_n)\langle\tau_a^z\rangle], \tag{69}$$

where $\langle\tau_a^z\rangle = \langle\chi_N^f(a)|\tau_a^z|\chi_N^i(a)\rangle$.

The NV$nda1$ terms are zero for $n>0$ because $e^{i\mathbf{q}\cdot\mathbf{r}_i}$ commutes with the static correlation operators. Also note that the exchange, NV$nea1$, terms are zero when $|\mathbf{k}_i|=|\mathbf{k}_f|$.

The NV$nxyz$ terms are given by

$$\mathrm{NV0}daz = \langle\tau_a^z\rangle, \tag{70}$$

$$\mathrm{NV1}djz = \int d^3r e^{-i\mathbf{q}\cdot\mathbf{r}} 2[(f^c-1)(\rho_p-\rho_n) + f^\tau\rho\langle\tau_a^z\rangle], \tag{71}$$

$$\mathrm{NV1}ejz = -\frac{1}{2}\int d^3r e^{i\mathbf{k}_i\cdot\mathbf{r}}\{(f^c-1+3f^\sigma+f^\tau+3f^{\sigma\tau}) \times(\rho_p\ell_p-\rho_n\ell_n) + (f^c-1+3f^\sigma+f^\tau+3f^{\sigma\tau}) \times(\rho_p\ell_p+\rho_n\ell_n)\langle\tau_a^z\rangle\}, \tag{72}$$

$$\mathrm{NV1}daz = 0, \tag{73}$$

$$\mathrm{NV1}eaNz = -\frac{1}{2}\int d^3r e^{i\mathbf{k}_f\cdot\mathbf{r}}\{(f^c-1+3f^\sigma+f^\tau+3f^{\sigma\tau}) \times(\rho_p\ell_p-\rho_n\ell_n) + (f^c-1+3f^\sigma+f^\tau+3f^{\sigma\tau}) \times(\rho_p\ell_p+\rho_n\ell_n)\langle\tau_a^z\rangle\}, \tag{74}$$

$$\mathrm{NV1}eaDz = \langle\tau_a^z\rangle \mathrm{NV1}eaD1, \tag{75}$$

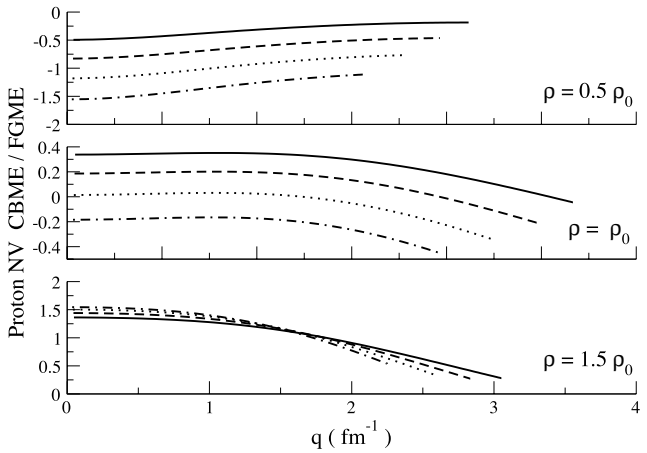

FIG. 10. Proton NV CBME scaled by FGME as a function of q and proton fraction x_p for $k_i = k_f = k_{Fp}$. The solid, dashed, dotted, and dash-dot lines show results for $x_p = 0.5,\ 0.4,\ 0.3,$ and 0.2.

$$\mathrm{NV2}djz = \int d^3r e^{-i\mathbf{q}\cdot\mathbf{r}}[(C_d^{00} - C_d^{11})(\rho_p - \rho_n) + 2(C_d^{10} + C_d^{11})\rho\langle\tau_a^z\rangle], \tag{76}$$

$$\mathrm{NV2}ejz = -\frac{1}{4}\int d^3r e^{i\mathbf{k}_i\cdot\mathbf{r}}\{(C_e^{00} + 2C_e^{10} + C_e^{11})(\rho_p\ell_p - \rho_n\ell_n) + (C_e^{00} + 2C_e^{10} + C_e^{11})(\rho_p\ell_p + \rho_n\ell_n)\langle\tau_a^z\rangle\}, \tag{77}$$

$$\mathrm{NV2}daz = \int d^3r[4C_d^{11}(\rho_p - \rho_n) - 4C_d^{11}\rho\langle\tau_a^z\rangle], \tag{78}$$

$$\mathrm{NV2}eaNz = -\frac{1}{4}\int d^3r e^{i\mathbf{k}_f\cdot\mathbf{r}}\{(C_e^{00} + 2C_e^{10} + C_e^{11}) \times (\rho_p\ell_p - \rho_n\ell_n) + (C_e^{00} + 2C_e^{10} + C_e^{11}) \times (\rho_p\ell_p + \rho_n\ell_n)\langle\tau_a^z\rangle\}, \tag{79}$$

$$\mathrm{NV2}eaDz = \langle\tau_a^z\rangle \mathrm{NV2}eaD1. \tag{80}$$

In symmetric nuclear matter the matrix elements of τ_z are related to those of $\tau^{\pm}$. In this case $\mathrm{NV}nxyz = Fnxy$. However, when $x_p < 0.5$ the NV matrix elements have additional terms dependent on $\rho_n - \rho_p$, or equivalently x_p.

Results of neutral-vector matrix element

In uncorrelated FG states, the neutral-vector matrix element is

$$-\sin^2\theta_W + \tfrac{1}{2}(1 - 2\sin^2\theta_W)\langle\tau_a^z\rangle = -0.2314 \pm 0.2686 \tag{81}$$

for the proton and neutron particle-hole pairs, respectively. The above two terms nearly cancel for uncorrelated protons. The correlations influence each operator differently and the final CB result depends sensitively on k_i, k_f, ρ, and x_p. The strong dependence of the proton NV matrix element on ρ and x_p is shown in Fig. 10 where we have plotted the proton particle-hole NV CBME scaled by 0.0372, the FGME. Note that the value of the CBME (not $|\mathrm{CBME}|^2$) is shown in this figure. At low densities the first term dominates, and the CBME is negative; however, at higher densities the second term becomes larger, and the matrix element becomes positive. At $\rho \sim \rho_0$ the cancellation of the two terms is almost exact, and the proton NV CBME is very small. Fortunately, in this case the FGME is small and the CBME is of the same order in the considered density range. Thus, the coupling of the proton NV current is not likely to have a significant contribution to the ν-nucleus interaction.

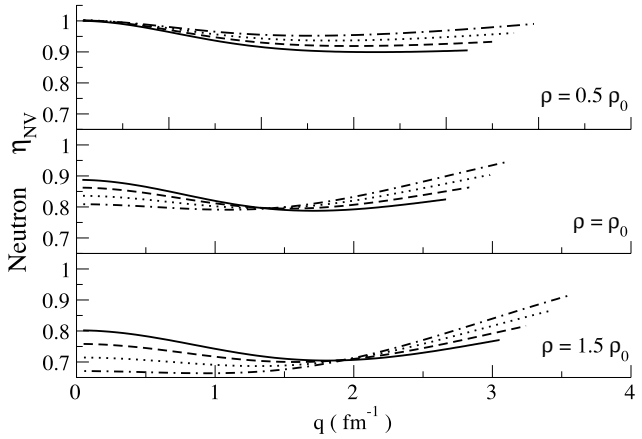

FIG. 11. Neutron η_{NV} as a function of q and proton fraction x_p for $k_i = k_f = k_{Fn}$. The solid, dashed, dotted, and dash-dot lines show results for $x_p = 0.5,\ 0.4,\ 0.3,$ and 0.2.

Figure 11 shows the density and x_p dependence of η_{NV} for neutron particle-hole pair excitations. At $\rho = \frac{1}{2}\rho_0$ the correlations increase the contribution of the first term and decrease that of the second term in Eq. (81) by a similar magnitude. Therefore at small ρ and q the NV neutron CBME $\sim$ FGME. However, at higher densities it is quenched. As mentioned earlier these matrix elements have a significant x_p dependence absent in the charge current matrix elements.

Figure 12 shows the contributions of the various correlations to the NV neutron CBME. The CBME is influenced by contributions of the $f^c - 1$ correlations to $\mathrm{NV}nxj1$ and those of the $f^{\sigma\tau}(r_{ij})\boldsymbol{\sigma}_i\cdot\boldsymbol{\sigma}_j\boldsymbol{\tau}_i\cdot\boldsymbol{\tau}_j$ and $f^{t\tau}(r_{ij})S_{ij}\boldsymbol{\tau}_i\cdot\boldsymbol{\tau}_j$ correlations to $\mathrm{NV}nxyz$ terms. The results obtained after setting $f^{\sigma\tau} = f^{t\tau} = 0$ and in addition $f^c = 1$ are shown by dashed and dash-dot lines in Fig. 12.

The neutral-vector CBME for a neutron particle-hole pair does not depend significantly on the magnitudes of the initial and final nucleon momenta. Variation of k_i from 0.5 to 1 and of k_f from $1k_F$ to $1.5k_F$ changes η_{NV} by less than 3%.

V. CORRELATED BASIS NEUTRAL-AXIAL-VECTOR MATRIX ELEMENT

The operator $\mathbf{O}_{NA}$ is an axial vector and it is convenient to express its matrix element using the following two axial vectors, similar to those used for the Gamow-Teller CBME (Sec. III):

$$\langle\boldsymbol{\sigma}_a\rangle = \langle\chi_N^f(a)|\boldsymbol{\sigma}(a)|\chi_N^i(a)\rangle \tag{82}$$

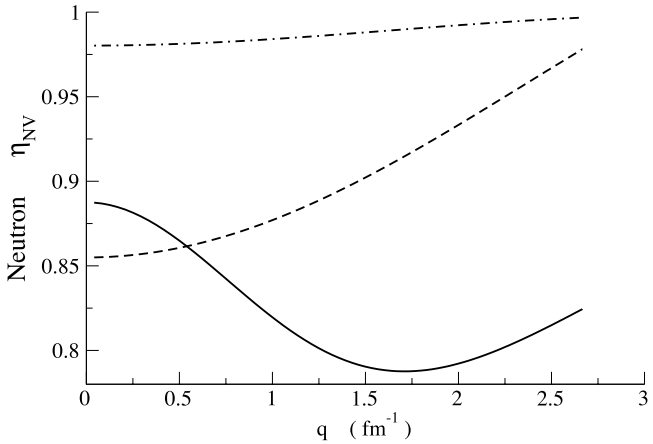

FIG. 12. Correlation dependence of the neutron η_{NV} for $k_i=k_f=k_{Fn}$ and $\rho=\rho_0$. The dashed line shows results with $f^{\sigma\tau}=f^{t\tau}=0$, and in addition, $f^c=1$ for the dash-dot line. The solid line gives the full result.

and

$$\langle \mathbf{A}_t\rangle = 3\hat{\mathbf{r}}_{aj}\langle \boldsymbol{\sigma}_a\rangle\cdot\hat{\mathbf{r}}_{aj} - \langle \boldsymbol{\sigma}_a\rangle. \tag{83}$$

We assume that χ_N^i in Eq. (57) is spin up and calculate the sum of the square of the NA matrix element for the two final states with $\chi_N^f=\uparrow,\downarrow$ for both $N=n$ and p. The terms in the cluster expansion of the NA CBME are denoted by NAnxy as in Sec. II, and the factor g_A is omitted for brevity. We obtain

$$\mathrm{NA0}da = \tfrac{1}{2}\langle \boldsymbol{\sigma}_a\rangle\langle \tau_a^z\rangle, \tag{84}$$

$$\mathrm{NA1}dj = \frac{1}{2}\int d^3r e^{-i\mathbf{q}\cdot\mathbf{r}} 2[(\rho_p-\rho_n)(f^\sigma\langle \boldsymbol{\sigma}_a\rangle + f^t\langle \mathbf{A}_t\rangle) + \rho\langle \tau_a^z\rangle(f^{\sigma\tau}\langle \boldsymbol{\sigma}_a\rangle + f^{t\tau}\langle \mathbf{A}_t\rangle)], \tag{85}$$

$$\mathrm{NA1}ej = -\frac{1}{4}\int d^3r e^{i\mathbf{k}_i\cdot\mathbf{r}}\{[(f^c-1+f^\sigma+f^\tau-3f^{\sigma\tau})\langle \boldsymbol{\sigma}_a\rangle + (f^t+3f^{t\tau})\langle \mathbf{A}_t\rangle](\rho_p\ell_p-\rho_n\ell_n) + [(f^c-1+f^\sigma+f^\tau+5f^{\sigma\tau})\langle \boldsymbol{\sigma}_a\rangle + (f^t-f^{t\tau})\langle \mathbf{A}_t\rangle](\rho_p\ell_p+\rho_n\ell_n)\langle \tau_a^z\rangle\}, \tag{86}$$

$$\mathrm{NA1}da = 0, \tag{87}$$

$$\mathrm{NA1}eaN = -\frac{1}{4}\int d^3r e^{i\mathbf{k}_f\cdot\mathbf{r}}\{[(f^c-1+f^\sigma+f^\tau-3f^{\sigma\tau})\langle \boldsymbol{\sigma}_a\rangle + (f^t+3f^{t\tau})\langle \mathbf{A}_t\rangle](\rho_p\ell_p-\rho_n\ell_n) + [(f^c-1+f^\sigma+f^\tau+5f^{\sigma\tau})\langle \boldsymbol{\sigma}_a\rangle + (f^t-f^{t\tau})\langle \mathbf{A}_t\rangle](\rho_p\ell_p+\rho_n\ell_n)\times\langle \tau_a^z\rangle\}, \tag{88}$$

$$\mathrm{NA1}eaD = \frac{1}{2}\langle \boldsymbol{\sigma}_a\rangle\langle \tau_a^z\rangle \mathrm{NV1}eaD1, \tag{89}$$

$$\mathrm{NA2}dj = \frac{1}{2}\int d^3r e^{-i\mathbf{q}\cdot\mathbf{r}}\{[(F_{d,j}^{00,\sigma}-F_{d,j}^{11,\sigma})\langle \boldsymbol{\sigma}_a\rangle + (F_{d,j}^{00,A}-F_{d,j}^{11,A})\langle \mathbf{A}_t\rangle](\rho_p-\rho_n) + [(F_{d,j}^{10,\sigma}+F_{d,j}^{01,\sigma}+2F_{d,j}^{11,\sigma})\times\langle \boldsymbol{\sigma}_a\rangle + (F_{d,j}^{10,A}+F_{d,j}^{01,A}+2F_{d,j}^{11,A})\langle \mathbf{A}_t\rangle]\rho\langle \tau_a^z\rangle\}, \tag{90}$$

$$\mathrm{NA2}ej = -\frac{1}{8}\int d^3r e^{i\mathbf{k}_i\cdot\mathbf{r}}[\{(F_{e,j}^{00,\sigma}+3F_{e,j}^{10,\sigma}-F_{e,j}^{01,\sigma}+F_{e,j}^{11,\sigma})\times\langle \boldsymbol{\sigma}_a\rangle + (F_{e,j}^{00,A}+3F_{e,j}^{10,A}-F_{e,j}^{01,A}+F_{e,j}^{11,A})\langle \mathbf{A}_t\rangle\}\times(\rho_p\ell_p-\rho_n\ell_n) + \{(F_{e,j}^{00,\sigma}-F_{e,j}^{10,\sigma}+3F_{e,j}^{01,\sigma}+F_{e,j}^{11,\sigma})\times\langle \boldsymbol{\sigma}_a\rangle + (F_{e,j}^{00,A}-F_{e,j}^{10,A}+3F_{e,j}^{01,A}+F_{e,j}^{11,A})\langle \mathbf{A}_t\rangle\}\times(\rho_p\ell_p+\rho_n\ell_n)\langle \tau_a^z\rangle], \tag{91}$$

$$\mathrm{NA2}da = \frac{1}{2}\int d^3r[F_{d,j}^{10,\sigma}+F_{d,j}^{01,\sigma}+2F_{d,j}^{11,\sigma}-2(C_d^{01}-C_d^{11})]\times\langle \boldsymbol{\sigma}_a\rangle(\rho_p-\rho_n) + (F_{d,j}^{00,\sigma}-F_{d,j}^{11,\sigma}-C_d^{00}-3C_d^{11})\times\langle \boldsymbol{\sigma}_a\rangle\rho\langle \tau_a^z\rangle], \tag{92}$$

$$\mathrm{NA2}eaN = -\frac{1}{8}\int d^3r e^{i\mathbf{k}_f\cdot\mathbf{r}}[\{(F_{e,j}^{00,\sigma}-F_{e,j}^{10,\sigma}+3F_{e,j}^{01,\sigma}+F_{e,j}^{11,\sigma})\times\langle \boldsymbol{\sigma}_a\rangle + (F_{e,j}^{00,A}-F_{e,j}^{10,A}+3F_{e,j}^{01,A}+F_{e,j}^{11,A})\langle \mathbf{A}_t\rangle\}\times(\rho_p\ell_p-\rho_n\ell_n) + \{(F_{e,j}^{00,\sigma}+3F_{e,j}^{10,\sigma}-F_{e,j}^{01,\sigma}+F_{e,j}^{11,\sigma})\langle \boldsymbol{\sigma}_a\rangle + (F_{e,j}^{00,A}+3F_{e,j}^{10,A}-F_{e,j}^{01,A}+F_{e,j}^{11,A})\times\langle \mathbf{A}_t\rangle\}(\rho_p\ell_p+\rho_n\ell_n)\langle \tau_a^z\rangle], \tag{93}$$

$$\mathrm{NA2}eaD = \frac{1}{2}\langle \boldsymbol{\sigma}_a\rangle\langle \tau_a^z\rangle \mathrm{NV2}eaD1. \tag{94}$$

Results of neutral-axial-vector matrix element

We discuss only the sum of the $|\mathrm{CBME}|^2$ over the two final spin states because it is independent of the chosen spin quantization axis. This sum equals 3/4 for FGME. In the following we provide results for

$$\eta_{NA} \equiv \tfrac{4}{3}(|\langle F\uparrow|\mathbf{O}_{NA}|I\rangle|^2 + |\langle F\downarrow|\mathbf{O}_{NA}|I\rangle|^2). \tag{95}$$

The η_{NA} for neutron and proton particle-hole pairs are plotted in Figs. 13 and 14, respectively, for the considered density and proton fraction values. In these matrix elements $k_i=k_f=k_{FN}$.

The charge-changing and neutral-axial-vector operators ($\mathbf{O}_{GT}$ and $\mathbf{O}_{NA}$), appropriately scaled, can be interpreted as the three components of an isospin vector operator. In symmetric nuclear matter the expectation values of these three components are equal, as one cannot quantify the isospin axis. The stars in Figs. 13 and 14 are results obtained for η_{GT} for symmetric nuclear matter with equivalent initial and final momenta and densities. They are identical to those obtained for η_{NA} for both proton and neutron particle-hole pairs.

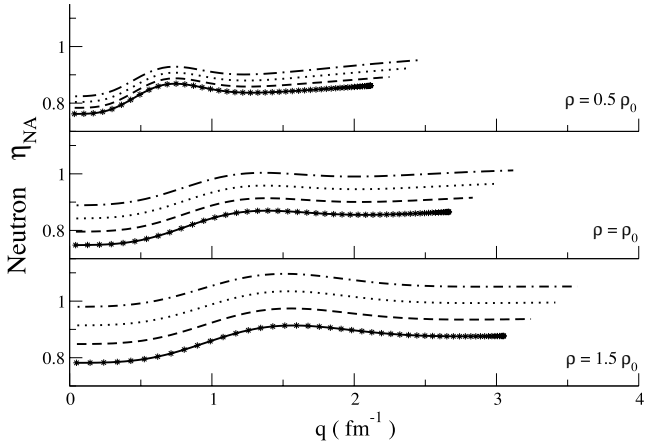

FIG. 13. Neutron η_{NA} as a function of q and proton fraction x_p for $k_i=k_f=k_{Fn}$. The solid, dashed, dotted, and dash-dot lines show results for $x_p=0.5$, 0.4, 0.3, and 0.2. The stars are results for η_{GT} at $x_p=0.5$.

Unlike the results for the GT CBME, there is a noticeable dependence of η_{NA} on the proton fraction at all densities considered. This $(\rho_p-\rho_n)$ dependence originates from the τ_j^z in NAnxj and NAnxa terms. We can approximate the NA results obtained for $x_p<0.5$ by adding a density dependent term proportional to $(\rho_p-\rho_n)$ to η_{NA} for symmetric nuclear matter. For small q, this approximation is

$$\eta_{NA}(\rho,x_p<0.5)=\eta_{NA}(\rho,x_p=0.5)-C_N(\rho)(\rho_p-\rho_n) \tag{96}$$

$$=\eta_{GT}(q=0)+\alpha_{GT}q^2-C_N(\rho)(\rho_p-\rho_n), \tag{97}$$

where we have used $\eta_{NA}=\eta_{GT}$ at $x_p=0.5$ and Eq. (40). The values obtained for $C_N(\rho)$ at the three densities considered are given in Table III.

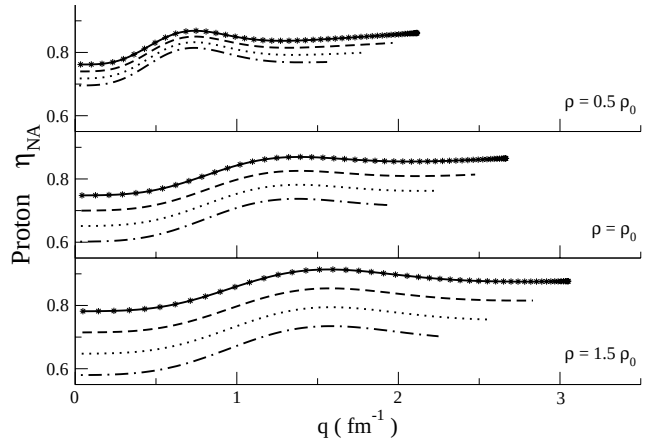

FIG. 14. Proton η_{NA} as a function of q and proton fraction x_p for $k_i=k_f=k_{Fp}$. The solid, dashed, dotted, and dash-dot lines show results for $x_p=0.5$, 0.4, 0.3, and 0.2. The stars are results for η_{GT} at $x_p=0.5$.

TABLE III. Linear fit to η_{NA} for $x_p<0.5$ at small q.

ρ	$C_p(\rho)$	$C_n(\rho)$
0.08	1.39	−1.29
0.16	1.53	−1.46
0.24	1.40	−1.38

The correlation dependence and the initial and final momenta dependences studied for η_{GT} are applicable here and will not be discussed further.

VI. CORRELATED BASIS INTERACTION

The expectation value of $H-T_{FG}(X)$, where $T_{FG}(X)$ is the kinetic energy of the Fermi-gas state Φ_X, is expanded to calculate the energy of the correlated state $|X\rangle$. It is given by

$$\langle X|H|X\rangle=\frac{\langle\Phi_X|[\mathcal{S}\Pi F_{ij}][H-T_{FG}(X)][\mathcal{S}\Pi F_{ij}]|\Phi_X\rangle}{\langle\Phi_X|[\mathcal{S}\Pi F_{ij}]^2|\Phi_X\rangle}+T_{FG}(X), \tag{98}$$

$$T_{FG}(X)=\sum_{\text{all } i \text{ occupied in } \Phi_X}\frac{k_i^2}{2m}. \tag{99}$$

Since Φ_X is an eigenstate of the kinetic energy operator $T=\Sigma_i-\nabla_i^2/2m$, with eigenvalue $T_{FG}(X)$, it is not necessary to expand the FG kinetic energy. $[H-T_{FG}(X)]|X\rangle$ does not contain terms with ∇_i^2 operating on $|\Phi_X\rangle$. Including only two-body clusters we obtain

$$\langle X|H|X\rangle=T_{FG}(X)+\sum_{i<j}\langle ij-ji|F_{ij}\Big[v_{ij}F_{ij}-\frac{1}{m}(\nabla^2F_{ij})-\frac{2}{m}(\boldsymbol{\nabla}F_{ij})\cdot\boldsymbol{\nabla}\Big]|ij\rangle, \tag{100}$$

where $|ij\rangle=e^{i(\mathbf{k}_i\cdot\mathbf{r}_i+\mathbf{k}_j\cdot\mathbf{r}_j)}\chi_\tau(i)\chi_\tau(j)$. The gradient operates on the relative coordinate, and the sum $i<j$ is over states occupied in Φ_X. The effective correlated basis two-nucleon interaction is given by [see Eq. (8)]

$$v_{ij}^{CB}=F_{ij}\Big[v_{ij}F_{ij}-\frac{1}{m}(\nabla^2F_{ij})-\frac{2}{m}(\boldsymbol{\nabla}F_{ij})\cdot\boldsymbol{\nabla}\Big] \tag{101}$$

in the two-body cluster approximation. The energies of correlated states $|X\rangle$ are obtained by using this v_{ij}^{CB} in first-order with FG wave functions Φ_X, as in the Hartree-Fock approximation.

The v_{ij}^{CB} has a momentum dependence via the $(\boldsymbol{\nabla}F_{ij})\cdot\boldsymbol{\nabla}$ term that gives contributions to the matter energy via exchange terms in Eq. (100). This contribution is much smaller than that of the momentum independent static terms in v_{ij}^{CB} defined as

$$v_{ij}^{CBS}=F_{ij}\Big(v_{ij}-\frac{1}{m}\nabla^2\Big)F_{ij}. \tag{102}$$

In the present work we have considered only the static part of F_{ij} as mentioned in the introduction. We therefore keep only the dominant static part of the full Argonne v_{ij}. The full v_{ij} is first approximated by a v_8' interaction chosen such that it equals the isoscalar part of the full interaction in all S and P waves as well as in the $^3D_1$ wave and its coupling to $^3S_1$. The difference between the full and the v_8' interactions is small and is treated perturbatively in the quantum Monte Carlo calculations [29]. v_8' has terms with the six static operators, $O_{ij}^{p=1,6}$, and two spin-orbit terms. The later two are omitted to obtain the static part of Argonne v_{ij}. In this approximation the v^{CBS} is a static operator having six terms with $O^{p=1,6}$:

$$v_{ij}^{CBS}=\sum_{p=1,6} v_p^{CBS}(r_{ij})O_{ij}^p. \tag{103}$$

The Landau-Migdal effective interactions used in studies of weak interactions in nuclei [14] and nucleon matter [7] are obtained from the spin-isospin susceptibilities of nucleon matter. We have therefore studied these susceptibilities with v^{CB} and v^{CBS}. The energy of nucleon matter with densities $\rho_{N\uparrow}$ and $\rho_{N\downarrow}$ can be expressed as

$$E(\rho,x,y,z)=E_0(\rho)+E_\tau(\rho)x^2+E_\sigma(\rho)y^2+E_{\sigma\tau}(\rho)z^2, \tag{104}$$

$$x=(\rho_{n\uparrow}+\rho_{n\downarrow}-\rho_{p\uparrow}-\rho_{p\downarrow})/\rho, \tag{105}$$

$$y=(\rho_{n\uparrow}-\rho_{n\downarrow}+\rho_{p\uparrow}-\rho_{p\downarrow})/\rho, \tag{106}$$

$$z=(\rho_{n\uparrow}-\rho_{n\downarrow}-\rho_{p\uparrow}+\rho_{p\downarrow})/\rho. \tag{107}$$

The τ, σ, and $\sigma\tau$ susceptibilities are proportional to $E^{-1}_{\tau,\sigma,\sigma\tau}$, and $E_0(\rho)$ is the energy of symmetric nuclear matter with $x=y=z=0$. Note that $E_\tau(\rho_0)$ is the familiar symmetry energy in the liquid drop mass formula. In principle, the above expansion is valid at small values of x, y, and z; however, within the accuracy of available calculations it seems to be valid up to $x=1$ [33,34].

We have calculated $E_{\tau,\sigma,\sigma\tau}(\rho)$ using the v^{CB} obtained from F_{ij} at $\rho=(\frac{1}{2},1,\frac{3}{2})\rho_0$. The results obtained with v^{CB} are given by full lines in Fig. 15, while those with the simpler v^{CBS} are given by dashed lines. The momentum dependent part of v^{CB} gives rather small contributions, which may be neglected in the first approximation. v^{CB} has a density dependence due to that of F_{ij}. However, it has very little effect on E_σ and $E_{\sigma\tau}$; the results obtained from the $(\frac{1}{2},1,\frac{3}{2})\rho_0 v^{CB}$'s essentially overlap. The density dependence of v^{CB} has a small but noticeable effect on the symmetry energy $E_\tau(\rho)$.

The stars on Fig. 15 show the values of $E_\tau(\rho)$ extracted from recent variational calculations [27] of symmetric nuclear matter (SNM) and pure neutron matter (PNM) with the Argonne-v18 and Urbana-IX interactions, assuming that Eq. (104) is valid up to $x=1$ for $y=z=0$. The two-body v^{CB} seems to provide a fair approximation to E_τ.

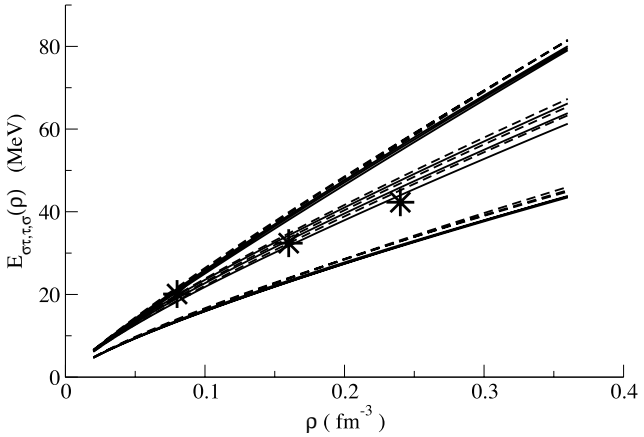

FIG. 15. $E_{\sigma\tau}(\rho)$ (upper set), $E_\tau(\rho)$ (middle set), and $E_\sigma(\rho)$ (lower set) of symmetric nuclear matter. In each set, the uppermost curves are results using F_{ij} for $\rho=\frac{1}{2}\rho_0$, the middle for $\rho=\rho_0$, and the lowest for $\rho=\frac{3}{2}\rho_0$. Solid lines show the results for v^{CB} and the dashed lines v^{CBS}. Stars denote values obtained for $E_\tau(\rho)$ from variational calculations [27].

We also consider the spin susceptibility of PNM given by the inverse of $E_\sigma^{PNM}(\rho)$ defined as

$$E^{PNM}(\rho,y)=E_0^{PNM}(\rho)+E_\sigma^{PNM}(\rho)y^2. \tag{108}$$

The results obtained with v^{CB} and v^{CBS} are shown in Fig. 16 along with those obtained from quantum Monte Carlo calculations [35] with the static parts of Argonne-v18 and Urbana-IX interactions. The two-body v^{CB}, using F_{ij} of SNM, gives fairly accurate values of E_σ^{PNM}.

Figure 17 shows $E_0(\rho)$ and $E_0^{PNM}(\rho)$ calculated from the v^{CB} at the three values of ρ. The stars in this figure give results of the recent variational calculations [27] with the full Argonne-v18 and Urbana-IX interactions. At low densities the two-body v^{CB} is not a bad approximation; however,

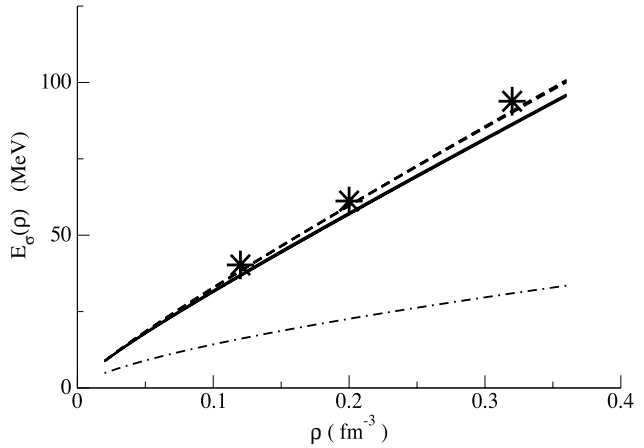

FIG. 16. $E_\sigma(\rho)$ for pure neutron matter. The solid line shows results obtained using v^{CB} and the dashed for the v^{CBS}. The results obtained with F_{ij} for $\rho=(\frac{1}{2},1,\frac{3}{2})\rho_0$ are essentially indistinguishable. Stars denote values obtained for $E_\sigma^{PNM}(\rho)$ from quantum Monte Carlo calculations [35]. The dash-dot line is the Fermi-gas $E_\sigma(\rho)$.

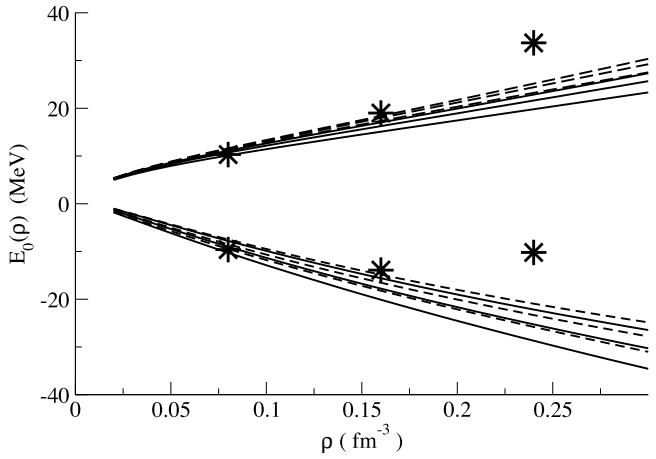

FIG. 17. $E_0(\rho)$ for symmetric nuclear matter (lower set of curves) and pure neutron matter (upper set of curves). In each set, the uppermost curves are results using F_{ij} for $\rho=\frac{3}{2}\rho_0$, the middle for $\rho=\rho_0$, and the lowest for $\rho=\frac{1}{2}\rho_0$. Solid lines show the results for v^{CB} and the dashed lines v^{CBS}. Stars denote values obtained for $E_0(\rho)$ from variational calculations [27].

$E_0(\rho)$ obtained from it does not show a minimum at ρ_0. The three-body interaction and cluster contributions are repulsive and are essential to obtain the minimum.

The two-body v^{CB} is more accurate in predicting the susceptibilities than the equation of state $E_0(\rho)$. This is partly because the contributions of T_{FG} and v^{CB} to $E_{\tau,\sigma,\sigma\tau}(\rho)$ add. The contribution of T_{FG} to E_σ^{PNM} is shown in Fig. 16 it is about half of the total. For this reason, even relatively simple estimates [36] of E_σ^{PNM} are not too different from the current state of the art [35]. In contrast, in SNM the large negative $\langle v^{CB}\rangle$ cancels T_{FG} to produce a relatively small binding energy. Therefore the many-body clusters are relatively more important in the calculation of $E_0(\rho)$.

The results of the recent SNM calculations, which provided F_{ij} used here, are summarized in Table IV. The one- and two-body cluster contributions are calculated exactly. The calculation of the three-body cluster contributions from the static part of F_{ij} are also exact. However, the three-body contributions from spin-orbit correlations and forces, the $n\geqslant 4$-body contributions and the difference between the variational and the ground state energies are estimated. The empirical $E_0(\rho)$ assumes $\rho_0=0.16$ fm^{-3}, $E_0(\rho_0)=-16$ MeV, and an incompressibility of 240 MeV. The difference between the calculated and the empirical values is likely to reduce when the more realistic Illinois V_{ijk} [30] is used in place of the Urbana-IX. However, a part of this difference is due to the approximations in the calculation.

TABLE IV. Contributions to the ground state energy of SNM from Argonne v_{ij} and Urbana V_{ijk} in MeV per nucleon.

Density (fm^{-3})	0.08	0.16	0.24
1-b T_{FG}	13.9	22.1	29.1
2-b all	−25.9	−43.7	−56.2
3-b static	4.9	10.9	19.1
3-b LS + $\geqslant$4−b all	−2.2	−1.7	0.8
(E_0-E_V)	−0.6	−1.8	−3.3
Calculated E_0	−9.9	−14.2	−10.6
Empirical E_0	−12.1	−16.0	−12.9

Next we consider the nondiagonal CB interaction. Let a Fermi-gas state $|\Phi_F\rangle$ differ from $|\Phi_I\rangle$ in the occupation numbers of two single-particle states:

$$|\Phi_F\rangle=a_n^\dagger a_m^\dagger a_j a_i|\Phi_I\rangle. \tag{109}$$

The matrix element of H between the CB states is given by

$$\langle F|H|I\rangle=\frac{\langle\Phi_F|[\mathcal{S}\Pi F_{ij}]H[\mathcal{S}\Pi F_{ij}]|\Phi_I\rangle}{\sqrt{\langle\Phi_F|[\mathcal{S}\Pi F_{ij}]^2|\Phi_F\rangle\langle\Phi_I|[\mathcal{S}\Pi F_{ij}]^2|\Phi_I\rangle}}. \tag{110}$$

The numerator of this matrix element contains terms in which the kinetic energy operator acts on Φ_I. These give

$$\frac{\langle\Phi_F|[\mathcal{S}\Pi F_{ij}][\mathcal{S}\Pi F_{ij}]T|\Phi_I\rangle}{\sqrt{\langle\Phi_F|[\mathcal{S}\Pi F_{ij}]^2|\Phi_F\rangle\langle\Phi_I|[\mathcal{S}\Pi F_{ij}]^2|\Phi_I\rangle}}=T_{FG}(I)\langle F|I\rangle. \tag{111}$$

When the correlated states are orthogonalized, this term is zero. Neglecting it the two-body cluster approximation of the above matrix element is obtained as

$$\begin{aligned}\langle F|H|I\rangle&=\langle mn|\left[v^{CBS}-\frac{1}{m}\{\boldsymbol{\nabla}'\cdot(F\boldsymbol{\nabla}')F+F(\boldsymbol{\nabla}F)\cdot\boldsymbol{\nabla}\}\right]|ij\rangle\\&=\langle mn|v^{CB}|ij\rangle.\end{aligned} \tag{112}$$

$\boldsymbol{\nabla}'$ operates to the left while $\boldsymbol{\nabla}$ to the right. When the momentum dependent term is negligible, this matrix is just the Fourier transform of v^{CBS}. Using the algebra of operators $O_{12}^{p=1,6}$ and Eqs. (102) and (103), we obtain

$$\begin{aligned}v_p^{CBS}=&\sum_{q,r,s,t=1,6}f^q v^r f^s K^{qrt}K^{tsp}-\sum_{q,s=1,6}\frac{1}{m}f^q\Bigg(\nabla^2-\frac{6}{r^2}(\delta_{s5}\\&+\delta_{s6})\Bigg)f^s K^{qsp}.\end{aligned} \tag{113}$$

Here we have used

$$\nabla^2 f^t(r_{ij})S_{ij}=S_{ij}\left(-\frac{6}{r_{ij}^2}f^t(r_{ij})+\nabla^2 f^t(r_{ij})\right) \tag{114}$$

and the K^{pqr} matrices are given in Ref [31]. The Fourier transforms of v_p^{CBS} are given in Figs. 18–20. Note that $S_{ij}=3\boldsymbol{\sigma}_i\hat{\mathbf{q}}\boldsymbol{\sigma}_j\hat{\mathbf{q}}-\boldsymbol{\sigma}_i\cdot\boldsymbol{\sigma}_j$ in momentum space.

The effective v^{CBS} is weaker than the bare v, particularly at large values of q, as shown in Figs. 18–20. Perturbative corrections typically involve a loop integration over the momentum transfer $\mathbf{q}$ with a q^2 phase-space factor. Hence in these figures we compare $q^2v_p^{CBS}(q)$ with $q^2v_p(q)$.

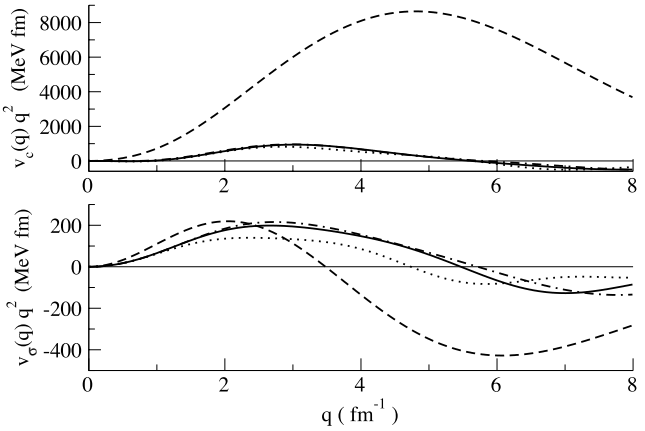

FIG. 18. The Fourier transform of the central and $\boldsymbol{\sigma}_i\cdot\boldsymbol{\sigma}_j$ components of v^{CBS} using F_{ij} obtained at $\rho=(\frac{1}{2},1,\frac{3}{2})\rho_0$ are shown by dotted, solid, and dash-dot lines, respectively. The dashed line shows the Fourier transform of the corresponding bare interaction.

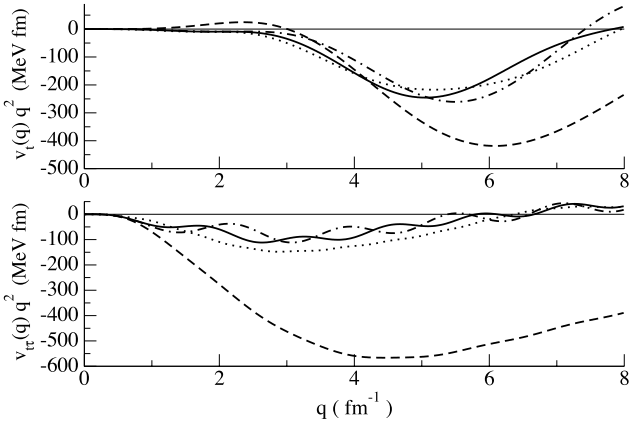

FIG. 20. The Fourier transform of the S_{ij} and $\boldsymbol{\tau}_i\cdot\boldsymbol{\tau}_j S_{ij}$ components of v^{CBS} using F_{ij} obtained at $\rho=(\frac{1}{2},1,\frac{3}{2})\rho_0$ are shown by dotted, solid, and dash-dot lines, respectively. The dashed line shows the Fourier transform of the corresponding bare interaction.

VII. CONCLUSIONS

We have calculated the effect of short-range correlations on nuclear weak interaction matrix elements. At low energies and small values of q, the charge current, weak transition rates are quenched by $\sim$20–25 % in the simplest two-body cluster approximation in the zeroth order CB theory. This quenching is relatively independent of the density and proton fraction of nucleon matter as well as the momenta of nucleons in the $(\frac{1}{2}-\frac{3}{2})\rho_0$ range. However, it depends on the momentum transfer q.

The dominant part of the quenching is due to spin-isospin correlations induced by the OPEP in the bare interaction. The OPEP changes the isospin of nucleons. For example, in the $n\rightarrow p$ weak transition between uncorrelated states the active nucleon is initially a neutron and finally a proton with unit probability. In correlated states, these probabilities are less than unit, and they reduce the weak interaction matrix elements. In particular, for the Fermi case, most of the q independent reduction is given by the product of the probabilities for the active quasinucleon to be initially a neutron and finally a proton. A similar interpretation is also applicable for the GT matrix elements.

In contrast to charge current, neutral-current matrix elements have a significant dependence on the proton fraction. The neutron-NV matrix element also depends on the total density, while the proton-NV matrix element is very small and varies with all relevant parameters.

We have also studied the effective nuclear interaction in the same CB used to calculate the weak interaction matrix elements. The dominant static part of the lowest-order two-body v^{CB} gives fairly accurate results for the spin, isospin, and spin-isospin susceptibilities of nucleon matter. However, it is necessary to include at least three-body effects to obtain the minimum in the $E_0(\rho)$ of symmetric nuclear matter. v^{CB} is much weaker than the bare v, and presumably can be used in perturbation theory formalism.

All calculations of weak transition rates using effective interactions must, in principle, use the quenched matrix elements calculated in the same basis. We plan to calculate the weak interaction rates in nucleon matter using the present effective operators and interactions. To obtain more accurate predictions, it will be necessary to include terms greater than equal to three-body terms in the cluster expansion of the CB effective operators and interactions.

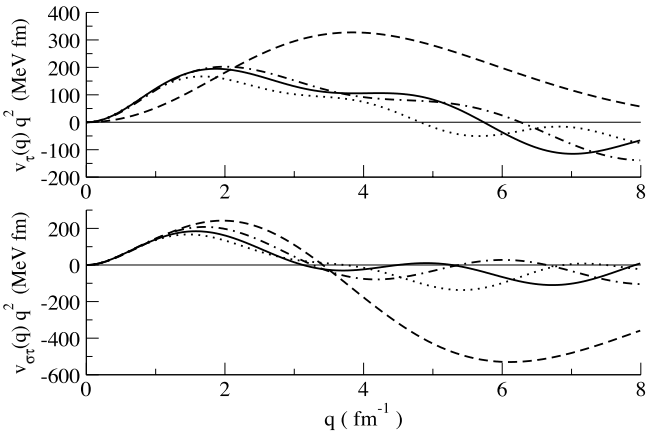

FIG. 19. The Fourier transform of the $\boldsymbol{\tau}_i\cdot\boldsymbol{\tau}_j$ and $\boldsymbol{\sigma}_i\cdot\boldsymbol{\sigma}_j\boldsymbol{\tau}_i\cdot\boldsymbol{\tau}_j$ components of v^{CBS} using F_{ij} obtained at $\rho=(\frac{1}{2},1,\frac{3}{2})\rho_0$ are shown by dotted, solid, and dash-dot lines, respectively. The dashed line shows the Fourier transform of the corresponding bare interaction.

ACKNOWLEDGMENTS

The authors would like to thank Dr. Chris Pethick, Dr. Sanjay Reddy, and Dr. Jochen Wambach for numerous discussions. This work was partially supported by the U.S. NSF via Grant No. PHY 00-98353.

APPENDIX A: SECOND-ORDER PERTURBATION THEORY

Standard perturbation theory is applicable when the bare interaction v_{ij} is weak. We then have $H=H_0+H_I$, $H_0=T$, and

$$H_I = \sum_{i<j} v_{ij}, \tag{A1}$$

Let $|\Phi_X\rangle$ be the unperturbed FG state. The perturbed, normalized state up to second order is given by

$$\begin{aligned}|X\rangle = &\left(1 - \frac{1}{2}\sum_{Y\neq X}\frac{|\langle\Phi_Y|H_I|\Phi_X\rangle|^2}{(E^0_{XY})^2}\right)\\ &\times\left(|\Phi_X\rangle + \sum_{Y\neq X}|\Phi_Y\rangle\frac{\langle\Phi_Y|H_I|\Phi_X\rangle}{E^0_{XY}}\right.\\ &+\sum_{Y,Z\neq X}|\Phi_Y\rangle\frac{\langle\Phi_Y|H_I|\Phi_Z\rangle}{E^0_{XY}}\frac{\langle\Phi_Z|H_I|\Phi_X\rangle}{E^0_{XZ}}\\ &\left.-\sum_{Y\neq X}|\Phi_Y\rangle\frac{\langle\Phi_Y|H_I|\Phi_X\rangle}{E^0_{XY}}\frac{\langle\Phi_X|H_I|\Phi_X\rangle}{E^0_{XY}}\right),\end{aligned} \tag{A2}$$

$E^0_{XY} = T_{FG}(X) - T_{FG}(Y)$. In this approximation the Fermi matrix element is given by $\langle F|O_F|I\rangle$, where Φ_I and Φ_F are given by Eq. (13).

We are concerned only with two-body effects and therefore consider only the interactions v_{aj} in H_I. The last two terms of the above $|X\rangle$ can be combined with the second by replacing v_{aj} by an effective interaction; hence we will omit them. The direct terms of $\langle F|O_F|I\rangle$ can be written as

$$\langle F|\sum_i O_F(i)|I\rangle_{direct} = F0da + F1dj + F2dj + F2da, \tag{A3}$$

since $F0dj$ and $F1da$ are zero. $Fnxy$ is defined as in Sec. II with the exception that n here refers to the order of H_I. We obtain

$$F0da = \langle \mathbf{k}_p|O_F(a)|\mathbf{k}_n\rangle = 1, \tag{A4}$$

$$\begin{aligned}F1dj = &\sum_{\mathbf{h}_N}\langle \mathbf{k}_p,\mathbf{h}_N|O_F(j)\frac{Q}{E_0-H_0}v_{aj}|\mathbf{k}_n,\mathbf{h}_N\rangle\\ &+\sum_{\mathbf{h}_N}\langle \mathbf{k}_p,\mathbf{h}_N|v_{aj}\frac{Q}{E_0+\omega-H_0}O_F(j)|\mathbf{k}_n,\mathbf{h}_N\rangle,\end{aligned} \tag{A5}$$

$$\begin{aligned}F2dj = &\sum_{\mathbf{h}_N}\langle \mathbf{k}_p,\mathbf{h}_N|v_{aj}\frac{Q}{E_0+\omega-H_0}O_F(j)\\ &\times\frac{Q}{E_0-H_0}v_{aj}|\mathbf{k}_n,\mathbf{h}_N\rangle,\end{aligned} \tag{A6}$$

$$\begin{aligned}F2da = &\sum_{\mathbf{h}_N}\left[\langle \mathbf{k}_p,\mathbf{h}_N|v_{aj}\frac{Q}{E_0+\omega-H_0}O_F(a)\frac{Q}{E_0-H_0}\right.\\ &\times v_{aj}|\mathbf{k}_n,\mathbf{h}_N\rangle - \frac{1}{2}\langle \mathbf{k}_p,\mathbf{h}_N|O_F(a)v_{aj}\frac{Q}{E_0-H_0}\\ &\times\frac{Q}{E_0-H_0}v_{aj}|\mathbf{k}_n,\mathbf{h}_N\rangle - \frac{1}{2}\langle \mathbf{k}_p,\mathbf{h}_N|v_{aj}\frac{Q}{E_0+\omega-H_0}\\ &\left.\times\frac{Q}{E_0+\omega-H_0}v_{aj}O_F(a)|\mathbf{k}_n,\mathbf{h}_N\rangle\right],\end{aligned} \tag{A7}$$

where $E_0 = e(\mathbf{k}_n) + e(\mathbf{h}_N), \omega = e(\mathbf{k}_p) - e(\mathbf{k}_n)$, Q is the projection operator to ensure Pauli exclusion in intermediate states, and $\mathbf{h}_N$ are any occupied proton or neutron states. We use $e(\mathbf{k})$ to denote single-particle energies; when $H_0 = T$, $e(\mathbf{k}) = k^2/2m$.

In order to make a connection with the correlated basis theory, we see that in perturbation theory the unnormalized two-body wave function is given by

$$|\Psi\rangle = \left(1 + \sum_{i<j}\frac{Q}{E_0-H_0}v_{ij}\right)|\Phi\rangle. \tag{A8}$$

Comparing it with the correlated wave function [Eq. (5)] we can identify

$$(F_{ij} - 1) \sim \frac{Q}{(E_0-H_0)}v_{ij} \tag{A9}$$

when the interaction is weak. In reality, v_{ij} is strong and Eq. (A9) is not useful. The correlation operator is determined variationally and its ω dependence is neglected assuming that the average value of $E_0 - H_0$ is much larger.

It can be verified that all of the $Fndy$ terms in Sec. II are obtained by replacing

$$\frac{Q}{E_0-H_0}v_{aj} \quad \text{and} \quad v_{aj}\frac{Q}{E_0+\omega-H_0} \tag{A10}$$

in Eqs. (A4)–(A7) by $(F_{aj} - 1)$, since $F^\dagger = F$.

APPENDIX B: THE *C* AND *F* COEFFICIENTS

The C parts required to calculate the effective weak vector operators in CB are obtained as follows: Let X, Y, Z be operators of type

$$X = \sum_{p=1,6} x_p O^p. \tag{B1}$$

The C part of the product of operators is then given by

$$C(XYZ) = \sum_{p,q=1,6}\sum_{r,s=1,6} x_p y_q z_r K^{pqs} K^{src}, \tag{B2}$$

where $O^c \equiv 1$ and the K^{pqr} are given in Ref. [31]. The results are listed below.

$$C^{11}_d = (f^\tau)^2 + 3(f^{\sigma\tau})^2 + 6(f^{t\tau})^2, \tag{B3}$$

$$C_d^{01}=C_d^{10}=(f^c-1)f^\tau+3f^\sigma f^{\sigma\tau}+6f^t f^{t\tau}, \quad \text{(B4)}$$

$$C_d^{00}=(f^c-1)^2+3(f^\sigma)^2+6(f^t)^2, \quad \text{(B5)}$$

$$C_e^{00}=(f^c-1)^2-3(f^\sigma)^2+12(f^t)^2+6(f^c-1)f^\sigma, \quad \text{(B6)}$$

$$C_e^{11}=(f^\tau)^2-3(f^{\sigma\tau})^2+12(f^{t\tau})^2+6f^\tau f^{\sigma\tau}, \quad \text{(B7)}$$

$$C_e^{01}=C_e^{10}=(f^c-1)f^\tau-3f^\sigma f^{\sigma\tau}+12f^t f^{t\tau}+3(f^c-1)f^{\sigma\tau}+3f^\sigma f^\tau. \quad \text{(B8)}$$

The $\boldsymbol{\sigma}_a$ and $\mathbf{A}_t$ parts of a product of $\boldsymbol{\sigma}_a\cdot\boldsymbol{\sigma}_j$, S_{aj}, $\boldsymbol{\sigma}_a$ and $\boldsymbol{\sigma}_j$ operators is obtained by repeated use of the Pauli identity:

$$\boldsymbol{\sigma}\cdot\mathbf{B}\boldsymbol{\sigma}\cdot\mathbf{C}=\mathbf{B}\cdot\mathbf{C}+i\boldsymbol{\sigma}\cdot\mathbf{B}\times\mathbf{C} \quad \text{(B9)}$$

to reduce it to terms linear in $\boldsymbol{\sigma}_a,\boldsymbol{\sigma}_j$. Terms linear in $\boldsymbol{\sigma}_j$ go to zero on summing over j. The remaining terms linear in $\boldsymbol{\sigma}_a$ are expressed in terms of the operators $\boldsymbol{\sigma}_a$ and $\mathbf{A}_t$ to obtain the following equations:

$$F_{d,a}^{00,\sigma}=(f^c-1)^2-(f^\sigma)^2-2(f^t)^2, \quad \text{(B10)}$$

$$F_{d,a}^{10,\sigma}=F_{d,a}^{01,\sigma}=(f^c-1)f^\tau-f^\sigma f^{\sigma\tau}-2f^t f^{t\tau}, \quad \text{(B11)}$$

$$F_{d,a}^{11,\sigma}=(f^\tau)^2-(f^{\sigma\tau})^2-2(f^{t\tau})^2, \quad \text{(B12)}$$

$$F_{d,a}^{00,A}=4f^\sigma f^t+2(f^t)^2, \quad \text{(B13)}$$

$$F_{d,a}^{10,A}=F_{d,a}^{01,A}=2f^\sigma f^{t\tau}+2f^t f^{\sigma\tau}+2f^t f^{t\tau}, \quad \text{(B14)}$$

$$F_{d,a}^{11,A}=4f^{\sigma\tau}f^{t\tau}+2(f^{t\tau})^2, \quad \text{(B15)}$$

$$F_{d,j}^{00,\sigma}=2(f^c-1)f^\sigma+4(f^\sigma)^2-4(f^t)^2, \quad \text{(B16)}$$

$$F_{d,j}^{10,\sigma}=F_{d,j}^{01,\sigma}=(f^c-1)f^{\sigma\tau}+f^\sigma f^\tau+2f^\sigma f^{\sigma\tau}-2f^t f^{t\tau}, \quad \text{(B17)}$$

$$F_{d,j}^{11,\sigma}=2f^\tau f^{\sigma\tau}+2(f^{\sigma\tau})^2-2(f^{t\tau})^2, \quad \text{(B18)}$$

$$F_{d,j}^{00,A}=2(f^c-1)f^t-2f^\sigma f^t+2(f^t)^2, \quad \text{(B19)}$$

$$F_{d,j}^{10,A}=F_{d,j}^{01,A}=(f^c-1)f^{t\tau}+f^t f^\tau-f^\sigma f^{t\tau}-f^t f^{\sigma\tau}+2f^t f^{t\tau}, \quad \text{(B20)}$$

$$F_{d,j}^{11,A}=2f^\tau f^{t\tau}-2f^{\sigma\tau}f^{t\tau}+2(f^{t\tau})^2. \quad \text{(B21)}$$

$$F_{e,a}^{00,\sigma}=(f^c-1)^2+2(f^c-1)f^\sigma+(f^\sigma)^2-4(f^t)^2, \quad \text{(B22)}$$

$$F_{e,a}^{01,\sigma}=(f^c-1)f^\tau-(f^c-1)f^{\sigma\tau}+3f^\sigma f^\tau+f^\sigma f^{\sigma\tau}-4f^t f^{t\tau}, \quad \text{(B23)}$$

$$F_{e,a}^{10,\sigma}=3f^{\sigma\tau}(f^c-1)+f^\tau(f^c-1)+f^{\sigma\tau}f^\sigma-f^\tau f^\sigma-4f^{t\tau}f^t, \quad \text{(B24)}$$

$$F_{e,a}^{11,\sigma}=2f^{\sigma\tau}f^\tau+(f^\tau)^2+(f^{\sigma\tau})^2-4(f^{t\tau})^2, \quad \text{(B25)}$$

$$F_{e,a}^{00,A}=2(f^c-1)f^t+2f^\sigma f^t+4(f^t)^2, \quad \text{(B26)}$$

$$F_{e,a}^{01,A}=2(f^c-1)f^{t\tau}-2f^\sigma f^{t\tau}+4f^t f^{\sigma\tau}+4f^t f^{t\tau}, \quad \text{(B27)}$$

$$F_{e,a}^{10,A}=-2f^{\sigma\tau}f^t+4f^{t\tau}f^\sigma+2f^\tau f^t+4f^{t\tau}f^t, \quad \text{(B28)}$$

$$F_{e,a}^{11,A}=2f^{\sigma\tau}f^{t\tau}+2f^\tau f^{t\tau}+4(f^{t\tau})^2, \quad \text{(B29)}$$

$$F_{e,j}^{00,\sigma}=(f^c-1)^2 2f^\sigma+(f^c-1)-4(f^t)^2+(f^\sigma)^2, \quad \text{(B30)}$$

$$F_{e,j}^{01,\sigma}=(f^c-1)f^\tau+3(f^c-1)f^{\sigma\tau}-f^\sigma f^\tau-4f^t f^{t\tau}+f^\sigma f^{\sigma\tau}, \quad \text{(B31)}$$

$$F_{e,j}^{10,\sigma}=f^{\sigma\tau}(f^c-1)+f^\tau(f^c-1)-4f^{t\tau}f^t+f^{\sigma\tau}f^\sigma+3f^\tau f^\sigma, \quad \text{(B32)}$$

$$F_{e,j}^{11,\sigma}=2f^{\sigma\tau}f^\tau+(f^\tau)^2-4(f^{t\tau})^2+(f^{\sigma\tau})^2, \quad \text{(B33)}$$

$$F_{e,j}^{00,A}=2f^t(f^c-1)+2f^\sigma f^t+4(f^t)^2, \quad \text{(B34)}$$

$$F_{e,j}^{01,A}=4f^\sigma f^{t\tau}+2f^t f^\tau-2f^t f^{\sigma\tau}+4f^t f^{t\tau}, \quad \text{(B35)}$$

$$F_{e,j}^{10,A}=2f^{t\tau}(f^c-1)+4f^{\sigma\tau}f^t-2f^{t\tau}f^\sigma+4f^{t\tau}f^t, \quad \text{(B36)}$$

$$F_{e,j}^{11,A}=2f^{\sigma\tau}f^{t\tau}+2f^{t\tau}f^\tau+4(f^{t\tau})^2. \quad \text{(B37)}$$

[1] SNO Collaboration, Q.R. Ahmad *et al.*, Phys. Rev. Lett. **87**, 071301 (2001).

[2] L.E. Marcucci, R. Schiavilla, M. Viviani, A. Kievsky, S. Rosati, and J.F. Beacom, Phys. Rev. C **63**, 015801 (2001).

[3] J. Kleinfeller *et al.*, in *Neutrino '96*, edited by K. Enquist, H. Huitu, and J. Maalampi (World Scientific, Singapore, 1997).

[4] L.B. Auerbach *et al.*, Phys. Rev. C **64**, 065501 (2001).

[5] L.B. Auerbach *et al.*, nucl-ex/0203011.

[6] *Proceedings of the First International Workshop on Neutrino-Nucleus Interactions (NuInt01)*, edited by M. Sakuda [Nucl. Phys. B (Proc. Suppl.) **112**, 1 (2002)].

[7] M. Prakash, J.M. Lattimer, R.F. Sawyer, and R.R. Volkas, Annu. Rev. Nucl. Part. Sci. **51**, 295 (2001).

[8] J.L. Forest, V.R. Pandharipande, S.C. Pieper, R.B. Wiringa, R. Schiavilla, and A. Arriaga, Phys. Rev. C **54**, 646 (1996).

[9] A. Akmal and V.R. Pandharipande, Phys. Rev. C **56**, 2261 (1997).

[10] R. Schiavilla *et al.*, Phys. Rev. C **58**, 1263 (1998).

[11] R. Schiavilla and R.B. Wiringa, Phys. Rev. C **65**, 054302 (2002).

[12] J.G. Congleton and E. Truhlik, Phys. Rev. C **53**, 956 (1996).

[13] A. Arima, K. Shimizu, W. Bentz, and H. Hyuga, Adv. Nucl. Phys. **18**, 1 (1987).

[14] E. Kolbe, K. Langanke, and P. Vogel, Nucl. Phys. **A652**, 91 (1999).

[15] A.C. Hayes and I.S. Towner, Phys. Rev. C **61**, 044603 (2000).

[16] K. Langanke, D.J. Dean, P.B. Radha, Y. Alhassid, and S.E. Koonin, Phys. Rev. C **52**, 718 (1995).

[17] G. Martinez-Pinedo, A. Poves, E. Caurier, and A.P. Zuker, Phys. Rev. C **53**, R2602 (1996).
[18] S. Reddy, M. Prakash, J.M. Lattimer, and J.A. Pons, Phys. Rev. C **59**, 2888 (1999).
[19] T.T.S. Kuo and G.E. Brown, Nucl. Phys. **A114**, 241 (1968).
[20] K. Suzuki and S.Y. Lee, Prog. Theor. Phys. **64**, 2091 (1980).
[21] P. Navratil, J.P. Vary, and B.R. Barrett, Phys. Rev. C **62**, 054311 (2000).
[22] S. Fantoni and V.R. Pandharipande, Nucl. Phys. **A473**, 234 (1987).
[23] S. Fantoni and V.R. Pandharipande, Phys. Rev. C **37**, 1697 (1988).
[24] J.W. Clark, Prog. Part. Nucl. Phys. **2**, 89 (1979).
[25] S. Fantoni, B.L. Friman, and V.R. Pandharipande, Nucl. Phys. **A399**, 51 (1983).
[26] A. Fabrocini and S. Fantoni, Nucl. Phys. **A503**, 375 (1989).
[27] J. Morales, V.R. Pandharipande, and G. Ravenhall, Phys. Rev. C **66**, 054308 (2002).
[28] R.B. Wiringa, V.G.J. Stoks, and R. Schiavilla, Phys. Rev. C **51**, 38 (1995).
[29] B.S. Pudliner, V.R. Pandharipande, J. Carlson, S.C. Pieper, and R.B. Wiringa, Phys. Rev. C **56**, 1720 (1997).
[30] S.C. Pieper, V.R. Pandharipande, R.B. Wiringa, and J. Carlson, Phys. Rev. C **64**, 014001 (2001).
[31] V.R. Pandharipande and R.B. Wiringa, Rev. Mod. Phys. **51**, 821 (1979).
[32] S. Fantoni and V.R. Pandharipande, Nucl. Phys. **A427**, 473 (1984).
[33] I.E. Lagaris and V.R. Pandharipande, Nucl. Phys. **A369**, 470 (1981).
[34] I. Bombaci and U. Lombardo, Phys. Rev. C **44**, 1892 (1991).
[35] S. Fantoni, A. Sarsa, and K.E. Schmidt, Phys. Rev. Lett. **87**, 181101 (2001).
[36] V.R. Pandharipande, V.K. Garde, and J.K. Srivastava Phys. Lett. **38B**, 485 (1972).